Received: 4 January 2023 | Revised: 9 April 2024 | Accepted: 30 April 2024

DOI: 10.1002/dep2.287

The Depositional Record Open Access
A journal of the International Association of Sedimentologists
WILEY

ORIGINAL RESEARCH ARTICLE

Chronostratigraphy and tectono-sedimentary history of the Eastern South Pyrenean foreland basin (Ripoll Syncline, North-East Spain)

Philémon Juvany[1,2] | **Miguel Garcés**[1,2] | **Miguel Lopez-Blanco**[1,2] | **Carles Martín Closas**[2] | **Elisabet Beamud Amorós**[1,3] | **Josep Tosquella**[4] | **Susanna Emilia Bekkevold**[1,2]

[1]Geomodels Research Institute, Universitat Barcelona, Barcelona, Spain

[2]Earth and Ocean Dynamics Department, Facultat de Ciències de la Terra, Universitat Barcelona, Barcelona, Spain

[3]Paleomagnetic Laboratory CCiTUB-ICTJA CSIC, Barcelona, Spain

[4]Departamento de Ciencias de la Tierra, Universidad de Huelva, Campus Universitario El Carmen, Huelva, Spain

Correspondence
Philémon Juvany, Geomodels Research Institute, Universitat Barcelona, Barcelona, Spain.
Email: pjuvany@ub.edu

Funding information
Marie Curie Project from the European Union, Grant/Award Number: H2020-MSCA-ITN-2019; Signal Propagation in Source to Sink for the Future of earth Resources and Energies (S2S-Future); PID2019-106440GB-C21 (Ministerio de Ciencia, Innovación y Universidades)

Abstract

This paper contributes to an understanding of the tectono-sedimentary evolution of the South Pyrenean foreland system by reviewing the chronostratigraphic framework of the basin infill in its eastern sector. Six sections are analysed and cross-correlated to build a 6.5 km thick composite magnetostratigraphy that represents the complete record of the Cadí Nappe in the Ripoll Syncline. New and previous magnetostratigraphic sections are integrated with available biostratigraphy to provide a new age calibration of the sedimentary succession of the Cadí Nappe, encompassing from Palaeocene to Middle Lutetian age. The proposed correlation with the Geomagnetic Polarity Time Scale aims at best reconcile magnetostratigraphic data with the regional biochronology built on the marine Shallow Benthic Zonation (SBZ biozones), the continental mammalian biochronology (MP levels) and the newly collected charophyte data. A subsidence analysis was performed on the calibrated composite succession, resulting in two well-defined intervals bounded by a hiatus. A Palaeocene to Early Eocene interval with low (11–21 cm/kyr) total subsidence rates, and an Early to Middle Eocene interval, characterised by high (70–75 cm/kyr) total subsidence rates. The detailed trends in both subsidence and sedimentation mark the development and evolution of the foreland depozones, from distal foreland depozones to foredeep and wedge-top depozones, relative to the emplacement of the Pedraforca Nappe and Cadí Thrust Nappe. The most pronounced sedimentary shift in the Cadí Nappe occurred at 49 Ma, with the rapid drowning of the carbonate platforms and its transition into talus and deep basinal environments. Carbonate platforms collapsed and resedimented on the talus of the elongated trough, newly formed parallel to the orogenic front. This marked the onset of tectonic subsidence triggered by the submarine emplacement of the Lower Pedraforca Nappe. The emersion of the orogenic wedge drove the entry of siliciclastics, lagged by 1 Myr, into the Ripoll

Trough. The foredeep filled rapidly (5.5 km thickness in less than 7 Myr) compared to other South Pyrenean regions, favoured by its semi-enclosed palaeogeography. The emplacement of the Vallfogona Thrust as early as the Middle Lutetian (43 Ma) brought the Cadi Nappe into a wedge-top setting. However, the Ripoll growth syncline continued acting as a temporary sink for alluvial sedimentation while a foredeep developed further south in the autochthonous Ebro Basin. The flexural response of the Iberian plate to the tectonic thickening of the Axial Zone counterbalanced for a period the local uplift of the Cadi Nappe, providing accommodation space for the top sediments filling the Ripoll Syncline.

KEYWORDS

biostratigraphy, chronostratigraphy, foreland basins, magnetostratigraphy, sedimentary provenance, sedimentary rates, sedimentology, source to sink, subsidence analysis, tectono-sedimentary evolution

1 | INTRODUCTION

Although the Cenozoic stratigraphy of the Pyrenees has been the focus of numerous studies, there remain strategic locations lacking a robust chronology. Assessing a detailed chronostratigraphic framework is crucial to understand the processes driving basin evolution and constitute an essential part of the source to sink approach. In the Pyrenees, the Early Eocene represents a debated stage of the evolution of the South Pyrenean Foreland, which is key to understand the evolution of the sediment transfer systems between the Eastern and Central South Pyrenean foreland in response to the tectonic emplacement of the Southern Pyrenean Central Unit. Detailed timelines are needed to set robust correlations and to assess the linkage between adjacent sedimentary systems.

Earlier magnetostratigraphic studies (Burbank et al., 1992; Vergés et al., 1998) aimed to provide absolute ages to the sedimentary successions of the South Eastern Pyrenean Foreland. Uncertainties remained in these pioneering studies due to either lack of sampling resolution or the lack of sufficient biostratigraphic constraints. This work seeks to refine key magnetostratigraphic sections to provide an accurate age model for Late Cretaceous to Middle Eocene deposits and propose a new correlation with the support of available and new biostratigraphic information. A new quantification of the sedimentation and subsidence is meant to lead us to a better interpretation of the tectono-sedimentary evolution of the foreland system.

2 | GEOLOGICAL SETTING

2.1 | The Eastern Pyrenees

The Pyrenean range is an east–west trending asymmetrical double-wedge continental orogenic belt resulting from the north-directed convergence between the Iberian and Eurasian plates (Choukroune, 1989; Muñoz, 1992; Vergés et al., 2002). Cross-sections based on seismic data (ECORS profile) show evidence that the Iberian plate has subducted under the Eurasian plate (Muñoz, 1992). Collision and partial subduction of the Iberian plate beneath the European plate lasted from the Late Santonian (Late Cretaceous) until the Oligocene–Early Miocene (Vergés et al., 1995). A southern pro-wedge thrust system developed on top of the subducting Iberian plate whereas a retro-wedge northern thrust system grew on top of the European plate (Vergés et al., 1995). A minimum total shortening of 111 km has been estimated for the Eastern Pyrenees by Grool et al. (2018). For the central part of the orogen a minimum shortening of 147 km has been estimated by Muñoz (1992), whereas a reduced shortening of 75–80 km was proposed by Teixell (1998) for the Western Pyrenees.

The Pyrenees can be divided into five structural units from south to north: (1) The Ebro Basin, the youngest and relatively undeformed pro-wedge foreland basin, sitting on autochthonous basement of the Iberian plate (Figure 1); (2) The South Pyrenean Zone (SPZ) is a fold and thrust belt that developed from Late Santonian to the Oligocene in a piggy-back thrust sequence over a Triassic salt decollement (Muñoz et al., 2018; Vergés et al., 2002); (3) The Axial Zone is a complex set of south-vergent thrust units mainly made of Hercynian basement rocks arranged in an antiformal stack connected to the SPZ thrusts (Choukroune, 1989; Muñoz, 1992); (4) The North Pyrenean Zone (NPZ), a narrow retro-wedge fold and thrust belt that involves pre-Alpine Palaeozoic massifs and inverted Mesozoic pre-orogenic rift-related stratigraphic successions (Ford et al., 2016); and (5) The Aquitaine foreland basin, the retro-wedge foreland basin located between the Pyrenees and the Massif Central.

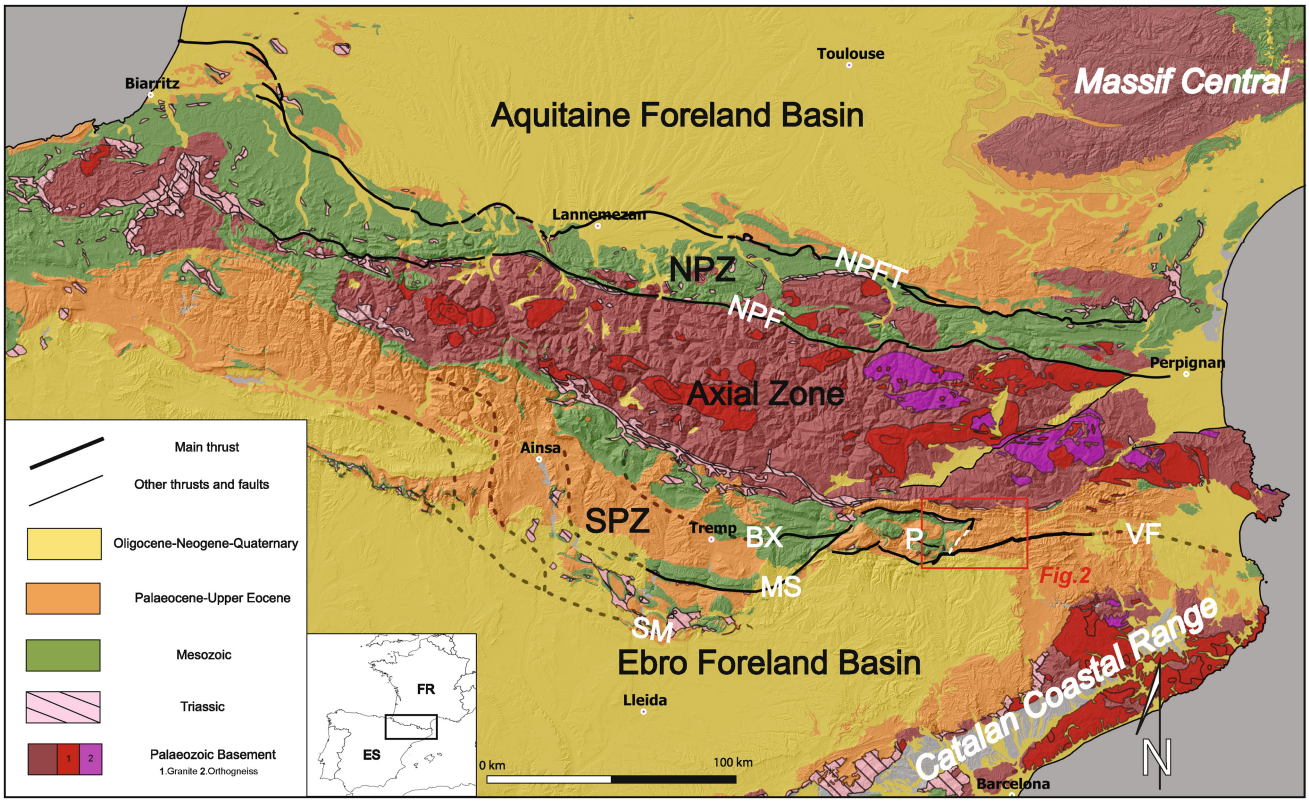

FIGURE 1 A geological map of the Pyrenees and adjoining areas, showing the main structural zones. Red square represents the position of Figure 2. B, Bóixols Thrust; MS, Montsec Thrust; NPF, North Pyrenean Fault; NPFT, North Pyrenean Frontal Thrust; NPZ, North Pyrenean Zone; P, Pedraforca unit. SPZ, South Pyrenean Zone; SM, Serres Marginales Thrust. Information extracted from IGME and BRGM shapefiles at 1:1,000,000 and 1: 250,000 scale.

The late Santonian to Oligocene evolution of the Southern Pyrenean fold and thrust belt underwent three different episodes of shortening related to the progressive emplacement of the different nappes, which from north to south in the central Pyrenees are: Bóixols, Montsec and Serres marginals. (Figure 1; Muñoz et al., 2018). These have their counterparts in the Eastern Pyrenees in the Upper, Middle and Lower Pedraforca nappes, which are respectively equivalent to Bóixols, Montsec and Serres marginals (Muñoz et al., 2018). The Vallfogona Thrust, carrying the Cadí Nappe and the Pedraforca Nappe on top, is the main boundary between the SPZ and the Ebro foreland basin in the Eastern Pyrenees.

The Upper Pedraforca Nappe, characterised by a thick Early Cretaceous succession, was emplaced between the Late Cretaceous and Palaeocene due to the inversion of rift-related normal faults, with average shortening rates that did not exceed 0.5 mm/year (Vergés et al., 1995). The Middle and Lower Pedraforca are mainly made of Late Cretaceous to Early Eocene rocks and were emplaced in the Early to Middle Eocene, with fast rates of shortening up to 4.5 mm/year (Vergés et al., 1995). The Cadí Nappe consists of a 2.5 km thick Palaeogene succession resting above Hercynian basement and thin Mesozoic cover. The hangingwall folding related to the Vallfogona thrust emplacement resulted in a 100 km long and 20 km wide syncline affecting the Cadi Thrust Sheet (Ripoll Syncline) and the Pedraforca Thrust Sheets. Deformation was also accommodated to the north by the growth of the antiformal stack affecting the hinterland Axial Zone at an average shortening rate of 2 mm/year (Vergés et al., 1995).

The so-called Ripoll sub-basin (Figure 2) formed as a narrow and elongated trough atop the Cadi Nappe (Vergés et al., 1995), and along the east–west-oriented Ripoll Syncline. It was partitioned from the undeformed South Pyrenean foreland during the emplacement of the Vallfogona Thrust in Middle Eocene times. To the north it is bounded by the Freser antiformal stack of the Axial Zone. The northern limb of the Ripoll Syncline includes more than 4 km of Late Cretaceous to Middle Eocene sediments. The succession forms a high angle ramp to flat geometry on the hangingwall of the Vallfogona Thrust (Figure 3). The southern limb contains 1.5 km of Middle Eocene sediments resting on a flat hangingwall contact on the Vallfogona Thrust (Ramos et al., 2002).

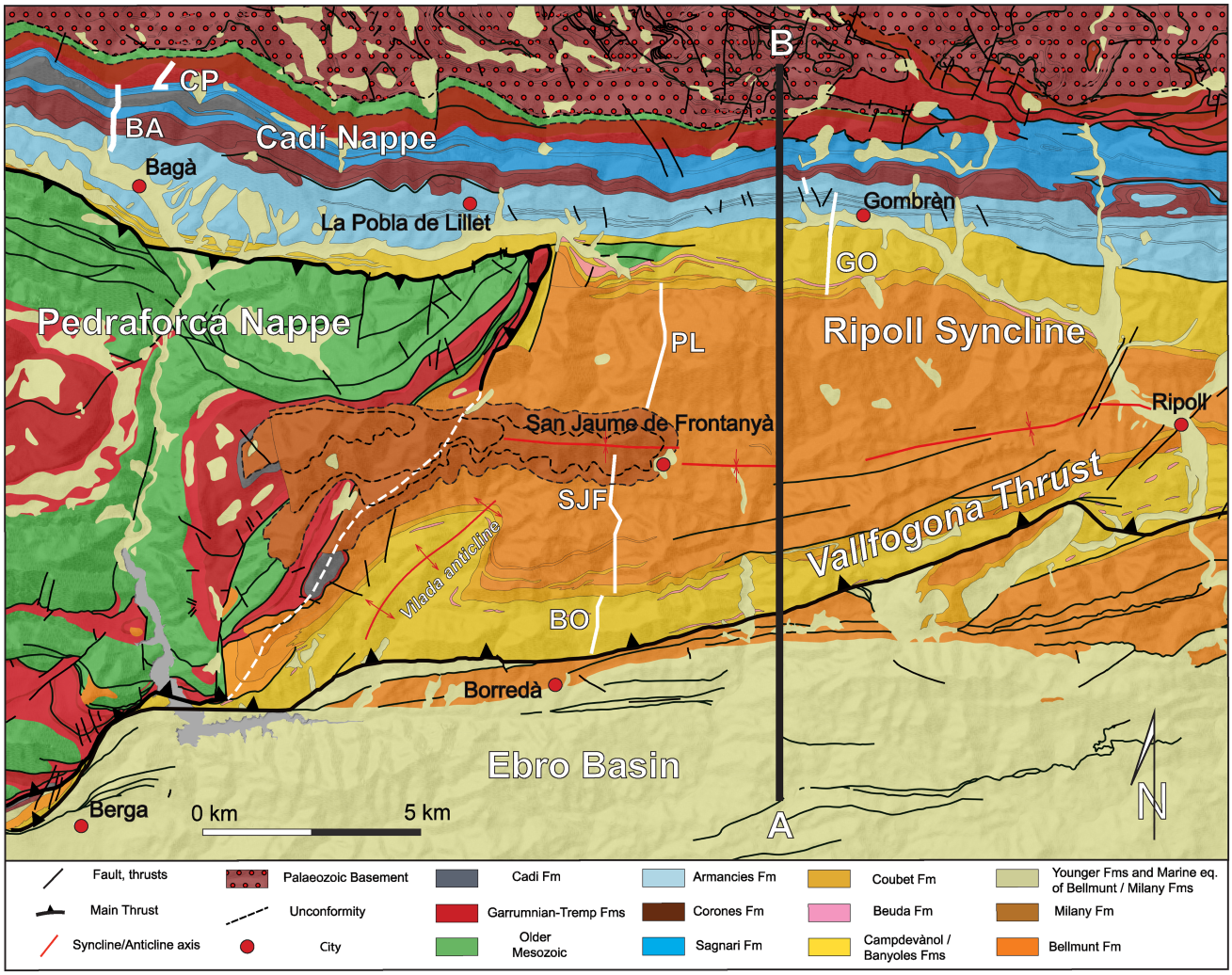

FIGURE 2 Geological map of the western Ripoll Syncline including the main structural and stratigraphic elements of the area. and the position of the studied sections (White lines). BA for Bagà, CP for Coll de Pal, GO for Gombrèn, PL for La Pobla de Lillet, BO for Borreda and SJF for Sant Jaume de Frontanyà. Modified from the Institut Cartogràfic i Geològic de Catalunya (ICGC) 1:50,000 scale shapefiles. EU-DEM Elevation model from The European Environment Agency.

2.2 | Stratigraphy of the Eastern Pyrenean foreland basin

The sedimentary wedge filling the Eastern Pyrenean foreland is characterised by strata thickening towards its northern active margin, and the southward displacement of facies and depocentres over time (Puigdefàbregas et al., 1986). From base to top, non-marine alluvial and lacustrine sediments (Garumnian facies) are overlain by shallow marine platforms (Cadí, Orpí, Peña, Tavertet formations) that grade northwards to deeper marine successions (Sagnari and Armancies formations) in an overall transgressive trend onto the southern margin. This, conjugated with a series of coeval progradational siliciclastic systems of northern provenance including turbiditic, fluvio-deltaic and alluvial fans sourced from the Pyrenees and the gradual stratigraphic onlap onto the southern foreland margin (Vergés et al., 1998) evidence the advance of the deformation front driven by plate convergence and underthrusting of the Iberian plate.

The pre-Cenozoic rocks of the Cadi Nappe consist of a thin Late Cretaceous transgressive–regressive succession (Figure 4) of shallow marine to lagoonal limestones, sandstones and mudstones that belongs to the Areny sequence (Simó & Puigdefàbregas, 1985), which lies unconformably above Triassic beds and Palaeozoic basement. This sequence starts with the transitional sediments of the Fumanya Member grading to the lagoonal Posa Formation (Vergés et al., 1994, Martínez et al., 2020; Oms et al., 2016). A depositional hiatus is observed at the base of the Fumanya Member and this formation appears brecciated due to emersion, indicating low subsidence

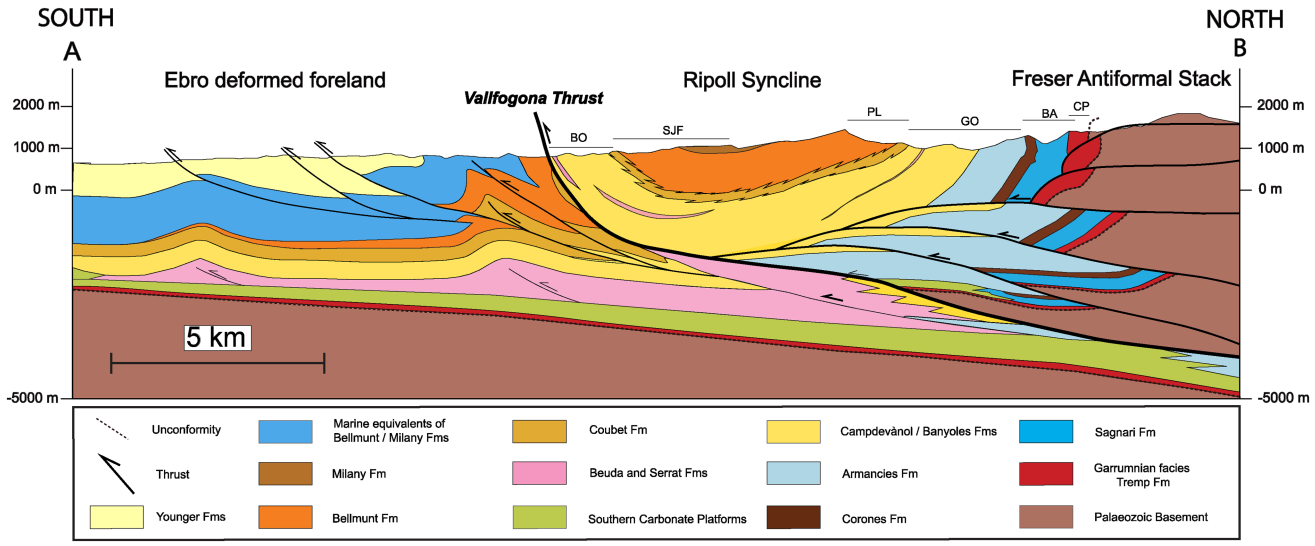

FIGURE 3 North–south cross-section of the South Eastern Pyrenees (position is drawn in white and named A–B on Figure 2) including the location of the studied sections (BA, Bagà; CP, Coll de Pal; GO, Gombrèn; PL, La Pobla de Lillet; BO, Borreda and SJF, Sant Jaume de Frontanyà). Modified from Bello et al. (2008) and Vergés (1993).

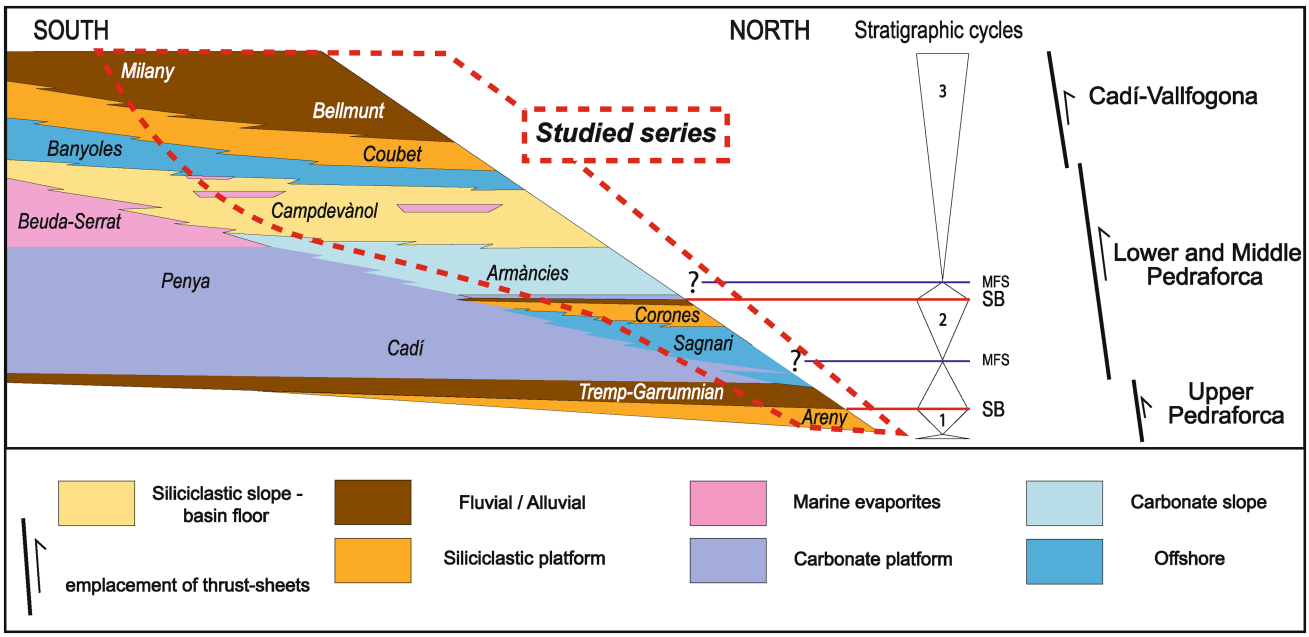

FIGURE 4 Stratigraphic chart of the study area including the transgressive–regressive cycles defined and the relationship between stratigraphic units and thrusting events. Modified from Vergés (1993), Bello et al. (2008) and Garcés et al. (2020).

and lack of accommodation space (Oms et al., 2016). The overlying succession is divided into 11 formal units, concisely described below:

The Tremp Formation, also known as the Garumnian, shows different characteristics according to the structural unit on which it was deposited. In the Vallcebre Basin (Lower Pedraforca Nappe), the Tremp Formation is divided into four members (Rosell & Llompart, 2001): (1) the grey Garumnian, composed of grey clays, lignites and interbedded sandstone and limestones deposited in a proximal marine environment; (2) the lower red Garumnian, made of fluvial palaeosol-bearing red mudstones and sandstones; (3) the Vallcebre limestone, composed of a massive unit of micritic lacustrine limestone rich in charophytes; (4) the upper red Garumnian is constituted of red palaeosoil-bearing mudstones, sandstones and lacustrine limestones with charophytes. The grey and lower red Garumnian are dated to the Maastrichtian in the Vallcebre Basin, and the Vallcebre limestone to the Danian (Oms et al., 2007). The age of upper red Garumnian is not

very well constrained, but since it is stratigraphically located between the Danian Vallcebre limestone and the Early Eocene marine formations, its age would span from Danian to the earliest Eocene. In the Tremp sub-basin, the upper red Garumnian contains the well-identified Claret conglomerate that is interpreted as the PETM locality (Domingo et al., 2009) and could also contain the Palaeocene–Eocene boundary in the Ripoll sub-basin.

In the Cadí Nappe, on the northern limb of the Ripoll Syncline, the Tremp Formation consists of a succession of about 300 m, which includes: (1) a lower unit made by channel, overbank and debris flow deposits with a fining upwards trend and corresponding to proximal alluvial fan deposits; (2) a middle unit made of floodplain clays silts, sandstones and lacustrine limestones with abundant Microcodium, corresponding to distal alluvial fan deposits; and (3) an upper unit made of lacustrine and palustrine limestones. This vertical succession is interpreted by Van Eeckhout et al. (1991) as the evolution from alluvial fan to lacustrine environments. The top 30 m thick massive limestone was interpreted by others as equivalent to the Vallcebre limestone of the Lower Pedraforca Nappe (Gómez-Gras et al., 2016).

The Eocene succession of the Cadí Nappe (Puigdefàbregas et al., 1986 among others) starts with the Ypresian Cadí and Sagnari formations (350 m), which mark the shift into marine conditions of the foreland basin. The Cadí Formation is made of limestones and marly limestones with abundant alveolinids and nummulites (Tosquella & Samsó, 1996) deposited in a carbonate platform environment. This shallow marine environment is made up of marls and marly limestones with abundant nummulites and grades laterally, north-eastward and upwards into deeper environments represented by the Sagnari Formation. It conformably overlies the Tremp Formation in the Bagà area and sandwiches the Cadí Formation. In the domain of the Lower Pedraforca Nappe, Ypresian sediments consist southward of platform to lagoonal carbonates and deeper mudstones, similar to the Cadí Formation (Vergés et al., 1994). Northward, to the Middle Pedraforca, they grade into siliciclastic shallow marine to fluvio-deltaic sediments in the Peguera Syncline (Martínez et al., 2020).

The Corones Formation (270 m) records a regressive sediment pulse followed by a transgressive event and includes siliciclastic and carbonate deposits. The Corones Formation is characterised by a southward prograding deltaic system initially deposited in a restricted marine environment indicated by Alveolina and Miliolidae faunal assemblages (Puigdefàbregas et al., 1986) grading upwards into shallow marine sandstones and finally into red beds with fluvial sandstones with southerly palaeocurrents (Puigdefàbregas et al., 1986). This continental member can be easily identified also with a grey carbonate bed rich in miliolids. The top part of the formation is made of laminated algal carbonates with abundant ostracods, miliolids, bivalves, gastropods and siliceous nodules (Tosquella & Samsó, 1996; Giménez-Montsant et al., 2002) indicating a deepening of the basin.

The Armàncies Formation (1000 m) is mainly made of carbonate slope deposits. The lower part consists of alternating marls and limestones with a high concentration of organic matter. The middle part is made of carbonate silts and breccias originating from the destruction of the carbonate shelf located upslope. It is admitted that resedimented carbonates in the Armàncies Formation could be derived from both northern and southern sources (Puigdefàbregas et al., 1986). The upper part is made of alternating marls and marly limestones with occasional bioclastic beds (Tosquella & Samsó, 1996). The Armàncies Formation is interpreted to mark the onset of the basin deepening triggered by the early basin flexural subsidence during thrust loading of the Pedraforca thrust sheets (Puigdefàbregas et al., 1986).

The siliciclastic turbidites of the Campdevànol Formation (900 m) overlie the Armancies Formation and represent an influx of terrigenous material in the basin. Slump folds and scars indicate southward dipping slopes, while palaeocurrents mark the dominant WSW axial transport, parallel to the trough (Puigdefàbregas et al., 1986).

The Beuda and Serrat formations were deposited during basin constriction and represent an evaporitic plug of varying geometry and thickness across the syncline. According to Puigdefàbregas et al. (1986), the restriction of the basin is attributed to the final emplacement of the Pedraforca Thrust Sheet. However, other studies (Bello, et al., 2008; Carrillo et al., 2014, 2017) consider Beuda and Serrat evaporites as southern time-equivalent deposits to the Campdevànol Formation.

The overlying formations are characterised by westward and later southward progradation of a thick fluvio-deltaic system with a series of laterally related formations (Banyoles, Coubet, Bellmunt and Milany formations). The vertical succession in the Ripoll Syncline starts with the prodelta marls of the Banyoles Formation (250–300 m; Puigdefàbregas et al., 1986). The delta-front sandstones of the Coubet Formation (250 m) progrades onto the Banyoles Formation and fossilise the Lower Pedraforca Thrust Sheet piggy-back sequence (Martínez et al., 1988). The delta plain to fluvial red beds of the Bellmunt Formation (1000 m; Ramos et al., 2002; Gich, 1973; Puigdefàbregas et al., 1986) hosts the mammal fossil-bearing sites of Sant Jaume de la Frontanyá I, II and III (Bonilla-Salomón et al.,2016). Topping the succession there are the proximal alluvial coarse sediments of the Milany Formation (400 m). An outstanding feature of the Milany Formation is that clast

composition shows an increasing proportion of basement pebbles suggesting exhumation of deeper structural levels in the tectonic pile of the Axial Zone (Freser antiformal stack; Ramos et al., 2002). Additionally, detrital zircon U–Pb–He double-dating data from Odlum et al. (2019) show a nearly unimodal Variscan (ca 300 Ma) U–Pb age distribution with zircon (U–Th)/He cooling ages all <70 Ma with an average of 53.8 ± 5.8 Ma, indicating exhumation from deep structural levels within the Variscan basement of the Freser antiformal stack (Axial Zone). Progressive unconformities on both flanks of the Ripoll Syncline indicate that sedimentation of the Milany Formation was coeval with the growth of the Freser antiformal stack and the displacement of the Cadí Nappe onto the Vallfogona Thrust footwall ramp (Martínez et al., 1988).

2.3 | Chronostratigraphic context

2.3.1 | Shallow Benthic Zones

A Biozonation was proposed for the Late Palaeocene–Early Eocene using larger foraminiferal biozones called 'Shallow Benthic Zones' (SBZ) in the work of Tosquella (1995). This proposal was made using the stratigraphic distribution of Nummulites sp., Assilina sp. and Alveolina sp. Further studies have refined the age boundaries of the SBZ (Pujalte et al., 2009; Rodríguez-Pintó et al., 2012; Serra-Kiel et al., 1998, 2020). The range of the SBZ within the sedimentary sequences of the Early Eocene in the Ripoll Basin have been described by Tosquella and Samsó (1996) and spans from SBZ5 (Ypresian) at the base of the marine succession to SBZ13 (Lutetian) at its top. The Cadí and Sagnari formations often yield species of different SBZ mixed, thus possibly indicating some reworking. Overall, these units range from SBZ5 to SBZ9, that is Ilerdian in age (Figure S1). The Corones Formation is assigned to the SBZ10, Early Cuisian. The slope sediments of the Armàncies Formation and turbidites of the Campdevanol Formation both contain fossils transported from the shallower platform environments, yielding mixed SBZ11 SBZ12 and SBZ13 elements, the youngest of these indicating the best guess of their depositional age. Finally, a short marine transgression interbeded within the lower Bellmunt Formation yielded the youngest larger foraminifera assemblage of the studied record, again assigned to SBZ13.

2.3.2 | Mammal biostratigraphy

Mammals are used as a tool for the establishment of biostratigraphic timescales in continental deposits during the Cenozoic. One of the most significant systems for the Palaeogene biostratigraphic subdivision is the Mammal Palaeogene (MP) reference levels. These levels are used in the same way as assemblage biozones although they represent specific faunas restricted in time and space (Bonilla-Salomón et al., 2016). In the southern flank of the Ripoll Syncline, the Bellmunt Formation outcrops at the locality of Sant Jaume de Frontanyà, which includes four fossil-bearing levels with an extraordinary abundance of mammal remains in a fine-textured fluvial and palustrine stratigraphic succession (Busquets et al., 1992; Moyà-Solà & Kohler, 1993). These findings indicate a Middle Eocene age based on their close affinity with faunas of Chéry-Chartreuve (Bonilla-Salomón et al., 2016), the proposed reference locality of MP15 (Comte et al., 2012). The MP15 faunas are classically correlated with the Early Bartonian stage based on regional stratigraphic marine–continental correlations in the Paris Basin.

2.3.3 | Previous Magnetostratigraphic studies

Earlier pioneering studies of Burbank et al. (1992) and Vergés et al. (1998) proposed magnetostratigraphic correlations for the Palaeogene sedimentary successions in the South Eastern Pyrenees foreland basin, but uncertainties remained due to either lack of sampling resolution, the need for further biostratigraphic constraints or the need for an improved laboratory method for sample analysis (applying a thermal demagnetisation adapted for each sample instead of a generalised protocol for a set of samples). The age obtained by these authors ranges between the Early Eocene and the Late Lutetian for the Palaeogene deposits of the Ripoll Syncline.

3 | METHODS

3.1 | Charophyte biostratigraphy

Charophyte samples were collected along the CP section. One sample was taken at the top of the underlying Cretaceous formation (According to the ICGC 1:50,000 map legends and Oms et al., 2016) while the six others were collected in the Garumnian red beds. The samples, usually 2–3 kg of rock (Figure S2), were obtained after systematic sampling of grey palustrine marls or claystones, presumably containing charophyte remains. The sediments were disaggregated in a solution of water, hydrogen peroxide (H_2O_2) and sodium carbonate (Na_2CO_3). After several days, the samples were wet sieved with mesh sizes of 1 mm, 500 µm and 200 µm. Once each residue had dried, charophytes were hand-picked under a Wild

M5A binocular stereomicroscope. Morphometric measurements were undertaken using Motic Images Plus 2.0 software. Selected gyrogonites were studied and photographed with a Quanta 200 scanning electron microscope at the Scientific and Technological Centres of the UB (CCiTUB). The material is housed in the charophyte collection of the Departament de Dinàmica de la Terra i de l'Oceà (Universitat de Barcelona).

3.2 | Magnetostratigraphy

A magnetostratigraphic study was carried out in the sections of Coll de Pal (CP), Baga (BA), Gombrèn (GO), La Pobla de Lillet (PL), Borreda (BO) and Sant Jaume de Frontanyà (SJF; Figures 2 and 3) to provide a reviewed age model of the Palaeocene–Eocene succession within the Ripoll Basin. The study focusses on providing higher resolution and robustness to earlier palaeomagnetic works made in the Ripoll Basin. Sampling was performed at regular stratigraphic intervals depending on the availability of required fine-grained sediments (silty and clayey materials). A resolution of one sample every 10 m was targeted, but this resolution was increased in the CP and BA sections (up to one sample every 3 m) and lowered depending on the outcrop quality. On the northern flank of the Ripoll Syncline a total of 382 palaeomagnetic sites were sampled spanning 5000 m. In the southern flank, a total of 226 samples were extracted spanning about 2900 m. In situ fresh and fine sediments were targeted to avoid remagnetisations caused by alteration or pedogenesis. Cylindric drill cores of an average length of 10 and 2.5 cm wide were extracted manually using a water-cooled portable electric powered drill and were oriented in situ using a special device made of mounted compass coupled with an inclinometer. Samples were prepared in the laboratory using a rotary saw to obtain the correct length accepted by the magnetometer (2.1 cm).

Magnetic measurements were conducted at the laboratory of palaeomagnetism housed in the Geo3BCN Institute (CCiTUB-CSIC) in Barcelona. The measurement of the natural remanent magnetisation was conducted using a three-axis superconducting rock magnetometer (2G-SRM750). To isolate the different magnetic components, samples were stepwise thermally demagnetised at 50°C and after at increments of 20°C after 400°C. Magnetic susceptibility was measured at each demagnetisation step with a KLY-2 (Geofyzica Brno) to track mineralogical changes upon heating.

The analysis of the Characteristic Remnant Magnetisation (ChRM) was based on visual inspection of Zijderveld plots and ChRM directions were calculated using principal component analysis. Possible viscous secondary components were excluded from the analysis. The ChRM components were ranked according to their quality. Class I refers to ChRM components showing small errors with linear nearly complete demagnetisation trends towards the origin of the diagram. Class II refers to ChRM components showing no increasing error while being demagnetised and a linear demagnetisation pointing towards the origin of the diagram. Class III corresponds to samples showing irregular demagnetisation trends or clustered direction not pointing towards the origin. Class III components were not considered further for magnetostratigraphic purposes.

Pmagpy software (Tauxe et al., 2016) was used to carry out the vector analysis. The distribution of ChRM components was analysed in both geographic and tilt-corrected coordinates at site level, and the mean inclination was corrected for flattening using the elongation/inclination (E/I) correction method (Tauxe et al., 2008). The age of the ChRM was further assessed by means of a regional fold test (Tauxe & Watson, 1994) at both sample and site levels.

The virtual geomagnetic pole (VGP) latitude was calculated for each ChRM direction and plotted against stratigraphic thickness to build a local composite magnetostratigraphy (LCM). Positive VGP latitudes were computed as normal polarity whereas negative VGP latitudes were computed as reversed polarity. Normal and reversed polarity magnetozones were defined for stratigraphic intervals having two or more consecutive samples of the same polarity. Correlation of the LCM with the Geomagnetic Polarity Time Scale (GPTS 2020; Gradstein & Ogg, 2020) was carried out after integration with relevant previous magnetostratigraphic data and existing and newly acquired marine and continental biostratigraphic data.

3.3 | Subsidence analysis

Subsidence analysis was carried out on the composite succession assuming a local isostasy model. The numerical age of formation boundaries was derived from interpolation of calibrated magnetostratigraphic boundaries. Formation and magnetostratigraphic boundaries combined were used to split the succession into units of known age and relatively homogeneous lithology and bathymetry. Decompacted thickness calculation was based on Van Hinte (1978) for changes in porosity with depth. Initial porosity and depth–porosity constant c were based on Sclater and Christie's (1980) values for terrigenous and carbonate sediments for evaporites. Palaeobathymetric values were taken from the study of Vergés et al. (1998). The minimum palaeobathymetries (palaeoaltitudes) proposed by Vergés et al. (1998) for the Bellmunt and Milany

formations have been modified to −300 m considering their horizontal distance to the time-equivalent coastal sediments and the approximate palaeoslopes following estimates of alluvial and fluvial gradients presented by Blair and McPherson (1994). Sea level from Miller et al. (2005) was used. The errors associated with porosities and compaction exponent c were not considered in the study. Tectonic subsidence was calculated by means of backstripping techniques based on Steckler and Watts (1978). Calculations assumed a density of 3.3 g/cm^3 for the asthenosphere and 1.0 g/cm^3 for the water.

4 | RESULTS

4.1 | ChRM characteristics and age of magnetisation

A total number of 608 samples were processed in the laboratory and subjected to stepwise thermal demagnetisation until complete removal of the NRM or reaching unstable behaviour. All the samples showed a low-temperature viscous component that was removed between 250 and 300°C. This component was directed towards the northeast or to the north possibly representing the present day magnetic field.

The ChRM components with dual polarity were often revealed at temperatures above 250–300°C, and maximum unblocking temperatures that were dependent on the lithology. Garumnian fluvial red beds lithologies from the Tremp Formation yielded unblocking temperatures around 660°C suggesting that haematite is the principal magnetic carrier. Red beds of the Bellmunt Formation, sampled in the PL and SJF sections yielded similar results. Lacustrine carbonates interbedded in the fluvial–alluvial facies of SJF, CP, BA and PL yielded unblocking temperatures below 600°C suggesting that magnetite minerals are the most abundant. Platform carbonates and lagoonal deposits of the Cadí and Corones formations demagnetised at *ca* 500–530°C suggesting that magnetite is the main magnetic carrier. The marlstone sediments from the deltaic Coubet and Banyoles formations and from outer platform deposits of the Sagnari Formation yielded unblocking temperatures between 300°C and 450°C. The organic matter-rich marlstone samples from the turbiditic series of Armancies and Campdevànol formations yielded unblocking temperatures between 350°C and 380°C before reaching unstable behaviour caused by the growth of new magnetic phases upon heating. In organic matter-rich sediments, iron sulphides can transform into magnetite during thermal demagnetisation, which would explain the sudden increase of magnetic susceptibility at temperatures above 380°C.

The ChRM directions were grouped into three classes according to their quality, resulting in 32.6% of Class I, 55.1% of Class II and 12.3% of Class III. The mean ChRM direction of each section was calculated from the set of samples of Class I and II, in both geographic and tectonic corrected coordinates. The mean Normal and Reversed polarity directions of all sections yielded a positive reversal test except for the BA section. The failed test in the BA section is interpreted to result from the inclination error of the remanence carried by haematite in the reversely magnetised Garumnian red beds, while the normally magnetised samples from overlying formations were much less affected by the shallowing bias.

A regional fold test was performed with the mean ChRM directions of the CP, BA, GO and PL sections, in the northern flank of the Ripoll Syncline, and BO and SJF in its southern flank. The fold test was done by flipping reversed polarity directions into their antipodal normal polarity direction and calculating an overall mean palaeomagnetic direction for each section. A stereonet plot of the mean directions in geographic coordinates (in situ) and stratigraphic corrected coordinates (bedding corrected) shows that directions tightly cluster around the overall mean after tectonic correction, thus suggesting that the magnetisation is prior to the folding of the Ripoll Syncline. A statistically significant positive fold test was obtained, with a best clustering at 105% unfolding, or 95% confidence bounds between 106% and 117% unfolding according to bootstrap foldtest (Tauxe & Watson, 1994). The overall mean direction after bedding correction was 356.0°/40.1° (dec/inc; Figure 5), which is significantly shallower than the expected 60° of inclination for the location of the northern Iberian plate in the Early Eocene (van Hinsbergen et al., 2020). But this anomalous inclination was corrected to a more consistent 51.2° after applying the (E/I) correction method (Tauxe et al., 2008). The northwards-directed mean direction indicates that no vertical-axis rotations occurred in this area after sedimentation of the study rocks.

A stepwise synfolding test was also applied, which consists of unfolding by steps of 5% from the total folding and looking at which percentage of unfolding the best statistic parameters are reached. Highest values of kappa and lowest values of alpha95 were obtained at *ca* 110% of unfolding (Figure 5), which are conclusive values for a positive fold test.

4.2 | Magnetostratigraphy

4.2.1 | Coll de Pal section

The Coll de Pal (CP) section is located on the northern flank of the Ripoll Syncline, along the road from Bagà to the Coll de Pal. It is approximately 300 m thick and

	Site	N	geographic coordinates Dg	Ig	k	α_{95}	stratigraphic coordinates Ds	Is	Is (E/I)	k	α_{95}
Bagà	BA	141	006.0	10.3	9.5	4.1	005.4	31.5	31.7	9	4.2
Coll de Pal	CP	128	357.3	-17.3	8	4.7	356.3	24.7	52.5	8.1	4.7
Pobla de Lillet	PL	21	005.6	-03.1	4.3	17.5	006.1	33.1	46.2	5.8	14.5
Gombren	GO	37	008.0	26.4	6.4	10.1	005.5	60.4	60.9	6.1	10.4
Borredà	BO	31	227.6	79.3	7.1	10.4	331.8	50.1	66.5	7.4	10.2
S. Jaume Frontanyà	SJF	176	337.7	76.4	8.9	3.8	347.8	37.3	46.4	9.7	3.6
All sites		**6**	**000.8**	**29.7**	**3.3**	**43.5**	**356.0**	**40.1**	**51.2**	**24.2**	**13.9**

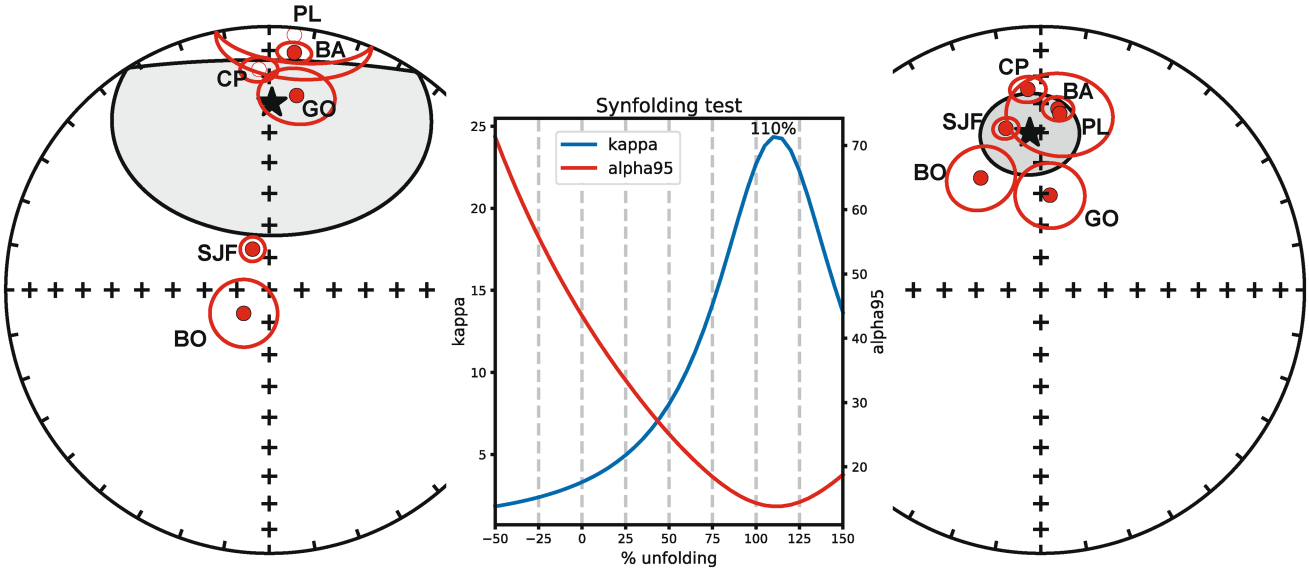

FIGURE 5 Mean palaeomagnetic directions and Fisher statistics at section level and the overall mean in geographic and (tilt-corrected) stratigraphic coordinates. Mean directions were corrected for inclination error using the E/I method of Tauxe et al. (2008). Stepwise unfolding yielded best kappa and α95 Fisher parameters after 110% unfolding (see text for discussion).

spans the whole outcropping red Garumnian facies of the Tremp Formation. The section was sampled at less than 3 m stratigraphic intervals with a total number of 139 oriented palaeomagnetic drill core samples. It directly starts 10 m above the youngest stratigraphic horizon showing Late Cretaceous rudist fossils and the first sample is taken directly within the first outcropping red bed layer. The top of the CP section is marked by a 30 m thick lacustrine limestone that forms a topographic relief easily mappable across the area. The average bedding dip of the sampled interval is 190°/42° (dip direction/dip).

The magnetic polarity of the CP samples is predominantly reverse (Figures S3 and S4). Only a few samples of normal polarity in the upper part of the section might represent two very short normal magnetozones in the upper part of the section, at 250 m and 290 m, but they represent very short intervals. These features are considered unreliable for correlation purposes, because the GPTS is not complete for very short geomagnetic reversals. They could be interpreted as possible recording of short geomagnetic features not yet calibrated in the time scale, or the product of an early diagenetic overprint. It is noteworthy, that in the laterally equivalent interval in the BA section no sign of a normal magnetozone was found.

Thus, the whole 300 m thick section of CP is interpreted as a unique reversed magnetozone. The obtained mean direction after bedding correction yielded an inclination (24.7°) heavily biased from expected geocentric axial dipole (GAD). This is interpreted to be a consequence of the combined effects of sedimentary and tectonic compaction. After applying the E/I correction method, a corrected inclination of 52.5° was obtained.

4.2.2 | Bagà section

The nearly 800 m thick Bagà (BA) section is located on the same road as the CP section, near the village of Gréixer. The lower 150 m consists of red Garumnian facies of the Tremp Formation, topped by the same thick limestone bed marking the top of the CP section. This mappable stratigraphic unit allows for a firm correlation between the CP and BA sections. The remaining 640 m of the BA section spans the entire Sagnari Formation, the Cadi Formation

and the Corones Formation. A total of 109 oriented palaeomagnetic drill core samples were sampled at a resolution of approximately 6 m. The average bedding dip of the sampled interval is 189°/42°, practically identical to the CP section.

In total, four reverse polarity magnetozones and three normal polarity magnetozones have been defined (Figures S5 and S6). The mean normal and reverse polarity directions fail to yield antipodal directions. This is interpreted to be a result of the combination of (a) inclination error that preferentially affects the reversely magnetised Garumnian facies, and (b) the contribution of a recent normal polarity partial overprint.

4.2.3 | Gombrèn section

The Gombrèn (GO) section is located on the northern flank of the Ripoll Syncline near the village of Gombrèn. Burbank et al. (1992) sampled the complete section that spans from the base of the Armancies Formation to the lower part of the Bellmunt Formation. Their results seemed coherent for most of the section except for the middle part, where the polarity reversals were supported by a limited number of samples. Therefore, efforts were focussed on a higher resolution sampling of the middle part of the GO section, which corresponds to the top of the Armàncies Formation, and includes the complete Campdevanol Formation The resampled interval starts at the hamlet called 'el Cortal' in the 'torrent de Puigbò', and comprises 65 oriented samples over a 1100 m stratigraphic interval, at a resolution of 17 m/site (Figures S7 and S8). The average bedding dip of the sampled interval is 191°/39°.

All the GO samples yielded normal polarity directions after bedding correction, except for one sample at 650 m, which was considered insufficient to represent a reliable magnetozone. Therefore, one normal magnetozone is defined in GO.

4.2.4 | La Pobla de Lillet section

The Pobla de Lillet (PL) section is located on the road from La Pobla de Lillet to Sant Jaume de la Frontanyà (SJF) and starts stratigraphically above the top of the Campdevanol Formation, overlying an evaporitic interval also traceable from the top of the resampled GO section. The 2500 m thick PL section spans the whole of the Coubet, Bellmunt and Milany formations and comprises 47 palaeomagnetic samples, taken at uneven sampling intervals that included large sampling gaps, these determined by outcrop access. The average bedding dip of the sampled interval is 180°/32°.

Both normal and reverse polarities were determined. Mean directions were relatively scattered but yielded inclination values closer to the expected Eocene reference after tectonic correction (Figures S9 and S10). Most of the section yielded a long interval of reversed polarity, followed by a short normal magnetozone over the top 200 m of the section. This single reversal is found to occur in the lower part of the Bellmunt Formation. In the transition interval from reverse to normal polarity, a series of sites of alternating polarities were not considered to provide a reliable record, and were possibly caused by post-depositional magnetisation that may affect the fluvial sediments of the Bellmunt Formation, also described in the SJF section below.

4.2.5 | Borredà section

The Borredà (BO) section is located on the southern flank of the Ripoll Syncline, along the road from Borredà to Sant Jaume de Frontanyà (Figures 2 and 3). The sampled section starts directly within the Campdevànol Formation, immediately north of the Vallfogona Thrust and in its hangingwall. The section comprises 51 oriented samples at a resolution of 15 m and is approximately 760 m thick. The average bedding dip of the sampled interval is 345°/45°.

Most of the samples yielded reversed polarity after tectonic correction that agreed with Eocene inclinations and appeared to be rotated 20° counterclockwise. Five samples yielded scattered normal polarity directions, with their mean in geographic coordinates close to present day field (Figures S11 and S12). After tectonic correction this direction is significantly biased from expected, with shallow inclinations and non-antipodal compared to the reversed polarity set. Therefore, those normal polarities are interpreted as a post-tilt normal overprint. The BO section is thus interpreted as a single reversed magnetozone.

4.2.6 | SJF section

This section is located on the southern flank of the syncline along the same road as the BO section. It is then the prolongation of the BO section into the Banyoles, Coubet, Bellmunt and Milany formations. This section is approximately 3100 m thick and includes the mammal localities of SJF-I, II and III. A total of 186 samples were collected from this section at an average resolution of 16 m. The northwards dip of beds decreases up-section from 40° to 20°, resulting in an average bedding dip of the sampled interval of 352°/36°.

The palaeomagnetic directions of the SJF section yielded antipodal normal and reverse polarities, and

closer to the expected GAD field after tectonic correction. The mean inclination, however, was slightly lower than expected for an Eocene palaeolatitude, partly corrected after applying the E/I correction method.

The SJF is divided into lower reverse and upper normal polarity magnetozones. The reversal occurs in a long transition interval characterised by a marked alternation of normal and reverse polarities. This record is interpreted to result from variably delayed magnetisation upon burial and compaction. Lithologies within the lower reversed magnetozone that experienced a greater lock-in depth picked the polarity of the overlying normal magnetozone (Figures S13 and S14). This artefact, which is not uncommon in magnetostratigraphic records, affected a very significant thickness of the SJF section. It can be explained in the context of very high sedimentation rates leading to burial of undercompacted sediments, increasing the depth at which the detrital remanent magnetisation is locked in. Under this scenario, the long transition interval is interpreted to be a consequence of primary reversed magnetisation, some levels being selectively remagnetised in normal polarity upon burial. Following this interpretation, the upper limit of the reverse magnetozone was placed at *ca* 550 m, the level of the uppermost reverse polarity samples.

Isolated samples of reverse polarity scattered within the upper normal magnetozone were not interpreted as reliable magnetozones and not considered for correlation purposes.

4.3 | Charophyte biostratigraphy

The CP section contains some poor assemblages of charophyte gyrogonites, which were found in samples CPCH-3 to CPCH-6. The following taxa were identified:

Sphaerochara edda (form A) Soulié-Marsche (1971; Figure S2A through F). Gyrogonites ($n = 32$ in CPCH-3) medium in size 475–500 μm high and 466–500 μm wide, subspherical in shape, with an isopolarity index (ISI = height × 100/width) of 98–100. Spiral cells, normally concave. About 8–11 cells are visible in lateral view. Apex rounded, sometimes with well individualised and poorly developed, apical nodules. Base rounded displaying a large, pentagonal basal plate visible from the outside.

Platychara aff. mucronata (Feist in Feist & Colombo, 1983; Vicente et al., 2016; Figure S2). The two gyrogonites available (sample CPCH-5) are large, 775–833 μm high and 625–650 μm wide, oblate, with an ISI of 75–83.8. Spiral cells concave, 5 or 6 visible in lateral view, separated by bicarinate sutures. Apex truncated, displaying a wide periapical depression, in the centre of which the apical cells raise to form a blunt prominence. Base truncated, ending in a short troncoconical pyramid, which displays a small basal pore.

Dughiella bacillaris (Feist-Castel, 1975; Figure S2). The single gyrogonite available (sample CPCH-6) is large, 583.3 μm high and 600 μm wide, spherical, with an ISI of 98. Seven spiral cells are visible in lateral view. They are concave and ornamented with characteristic vertical rods, regularly spaced, as high as the spiral cell width. Apex flat with slight apical thinning. Base slightly tapering, bearing a small apical pore.

Microchara cf. vestita (Castel, 1969; Figure S2). Gyrogonites ($n = 4$ from CPCH-3) small to very small, about 323–325 μm high and 250–258 μm wide, oval-shaped, with an ISI of 125–130. Up to nine concave spiral cells are visible in lateral view. Apex rounded and without any apical modification. Base tapers to end with a point that bears a small basal pore.

The lowermost sample CPCH-5 collected shortly below the studied Garumnian red beds in the late Cretaceous marine Areny sequence contains Platychara cf. mucronata and indicates a middle Maastrichtian to early Danian age (Vicente et al., 2019). The most abundant species encountered is Sphaerochara edda (form a), which has been identified throughout the section studied (samples CPCH-3 and CPCH-4). This species is Danian to Thanetian in age (Riveline, 1986). Sample CPCH-6 located approximately 80 m above the base of the Coll de Pal section contains Dughiella bacillaris, which gives a Danian to Early Thanetian age (Riveline, 1986). Finally, Microchara cf. vestita was located in the upper part of the Coll de Pal section, approximately 270 m from the base (sample CPCH-3), and gives a Thanetian–Ypresian age (Riveline, 1986). In sum, the age attributed by charophyte biostratigraphy to the Coll de Pal section ranges between Danian and Early Thanetian for the lower part, while the topmost part of the section would belong to the Thanetian–Ypresian.

5 | DISCUSSION AND IMPLICATIONS

5.1 | Magnetostratigraphy

5.1.1 | A local composite magnetostratigraphy

A LCM of the Ripoll Syncline succession was built based on the data provided in this study and earlier works (Burbank et al., 1992). A first-order chronostratigraphic scheme (Figure S15) is already available from the well-established lithostratigraphic subdivision and the biostratigraphic constraints provided preferentially from marine strata (Puigdefàbregas et al., 1986; Busquets

et al., 1992; Tosquella, 1995; Tosquella & Samsó, 1996; Ramos et al., 2002).

Along the northern flank of the Ripoll Syncline, the sections CP, BA, GO and PL combined provide a complete record of the Palaeogene stratigraphy from the Tremp Formation to the lower part of the Bellmunt Formation, and the substantial overlap between most of the sections ensures completeness of the resulting LCM. The CP and BA sections, which largely overlap at the level of the Tremp Formation, are merged into one single section (Figure 6). The correlation between BA and the GO section is based on the distinct expression of the Corones/Armancies formation boundary across the region, implying that the top reverse magnetozone in Bagà merges with the long lower reversed magnetozone in the GO section (R4 in Figure 6).

The sections on the southern flank (BO and SJF) allowed the record to be extended upwards into the Bellmunt Formation. Correlation between the northern and the southern flank is unambiguous given the proximity of the top SJF and PL sections, both converging towards the axis of the syncline in the vicinity of the Sant Jaume de Frontanyà (Figure 2), where beds are traceable across the fold axis (Martínez et al., 1988; Ramos et al., 2002). The proposed correlation reveals an important north–south diachrony (younging southwards) of the upper units, from the Campdevànol Formation to the Bellmunt Formation, as already pointed out by Ramos et al. (2002).

The correlation of all the sections results in a 6500 m thick LCM of the Ripoll Syncline that consists of five reverse and five normal polarity magnetozones. Compared to earlier magnetostratigraphic studies, this work identified in the BA section one normal magnetozone in the Sagnari Formation (N1 in Figure 6), which was previously overlooked (Burbank et al., 1992). On the other hand, three magnetozones reported in that earlier work are not confirmed in this study. First, a relatively thick (150 m) reversed magnetozone was interpreted by others in the middle of the Campdevànol Formation in the GO section (Burbank et al., 1992). The results of this study, however, reduced this to one single reversed polarity site

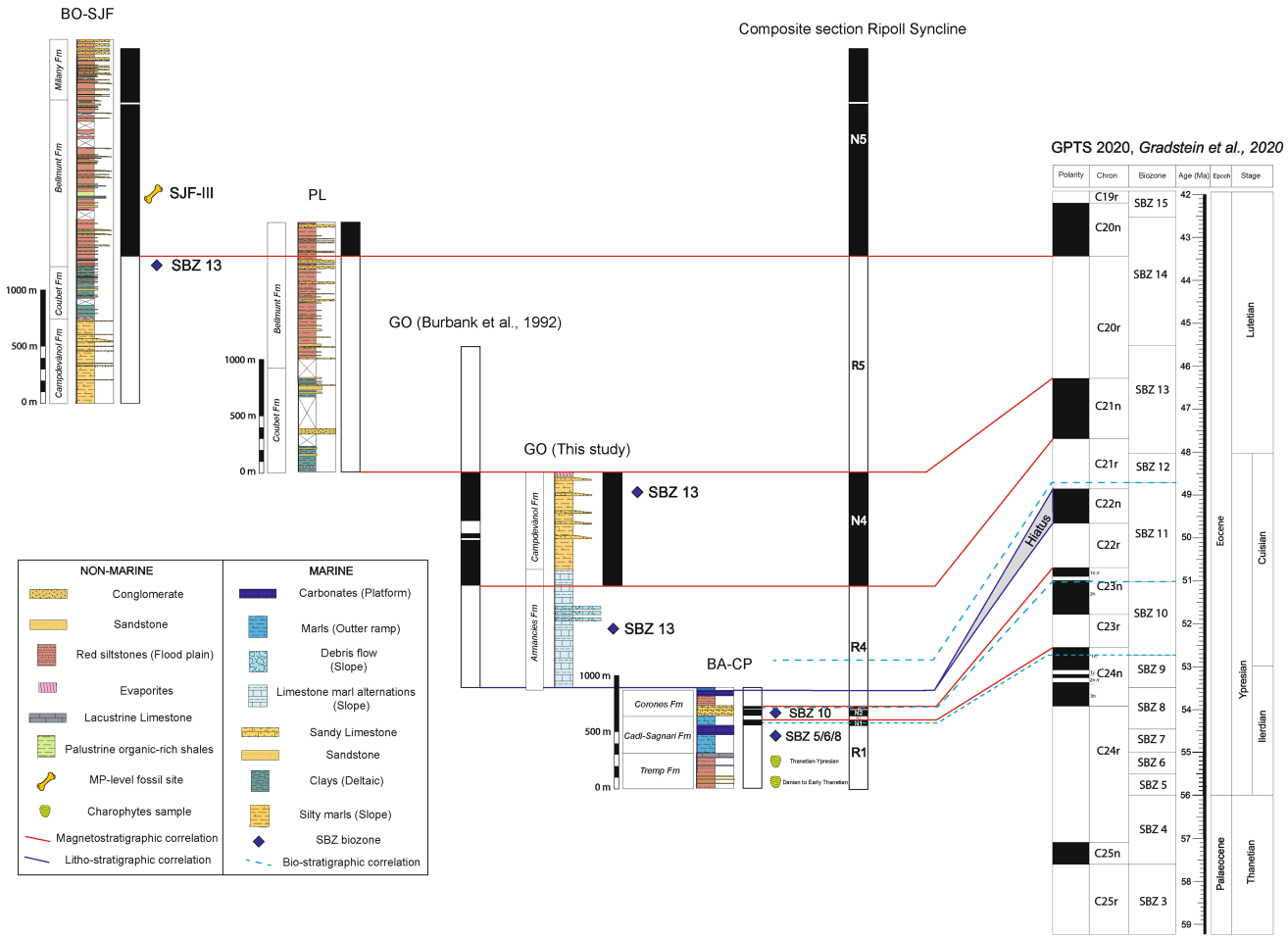

FIGURE 6 Composite Local Magnetic Polarity Stratigraphy (LMPS) of the Ripoll Syncline built from the correlation of the Borredà-Sant Jaume de Frontanyà (BO-SJF), LP (La Pobla de Lillet), GO (Gombren) and BA-CP (Bagà-Coll de Pal) sections. Right: Correlation of the LMPS with the GPTS 2020.

and therefore lacks significance for correlation purposes. Second, a very short normal polarity magnetozone was interpreted by Burbank et al. (1992) at the level of an evaporitic interval at the top of the Campdevànol Formation in the SJF–BO composite section. This record is thought unreliable since the evaporitic body probably represents an olistolith of Triassic evaporites brought to the basin floor by mass-gravity processes. Third, two consecutive sites at about the middle of the Bellmunt Formation in the SJF section led Burbank et al. (1992) to interpret a reversed magnetozone. Noticeably, this interval appears to coincide with a coal-bearing lacustrine unit interlayered with the red bed succession. In this study, one sample at the base of the lacustrine beds confirmed a reversed polarity magnetisation, but the concurrence of the reversal with referred sharp lithological contrast points to a post-depositional artefact. Organic-rich sediments are prone to bear unstable Fe-sulphides that later oxidise to magnetite or haematite giving rise to a secondary magnetisation. This observation, together with the fact that it relies on one single sample, suggests that this reversed magnetozone is unreliable.

5.1.2 | Biostratigraphic constraints

On the northern flank of the Ripoll Syncline, the charophytes of the sample CPCH5 (*Platychara mucronata*) strata underlying the CP section (and within the Areny sequence) are characteristic of Maastrichtian to Early Danian age. This is consistent with the biostratigraphic data from equivalent sections in the Ager and Tremp subbasins, which yield a Campanian–Maastrichtian age for the Fumanya Member (Oms et al., 2007). The analysis of charophyte assemblages have revealed an age range for the Tremp Formation in the CP section between Danian to Early Thanetian for the base of the section and Thanetian–Ypresian for the topmost part of the section.

The position of the SBZ biozones and fossil occurrences are summarised in Figure S2 using the data principally from Tosquella (1995). Within the Cadi and Sagnari formations, benthonic foraminifera assemblages range from SBZ5 to SBZ9. Considering the reworking of fossils, the depositional age of the sampled localities can be constrained to range from SBZ7 to SBZ9. The lowermost shallow marine Corones Formation includes fauna from SBZ10. In the overlying Armàncies and Campdevànol formations, larger foraminifera are transported, and taxa representative of SBZ11 and SBZ12 are found mixed with SBZ13 assemblages. SBZ13 is also identified within the last marine incursion of the Coubet Formation in the lower Bellmunt Formation at the SJF section (Ramos et al., 2002; Tosquella & Samsó, 1996; Busquets et al., 1992).

Recent work has been done on the uppermost level of Sant Jaume de Frontanya-1 (SJF-I) and has led to the identification of three different forms of rodents, giving more primitive forms than the Late Bartonian (MP16) localities and thus attributing an age corresponding to the Early Bartonian (MP15) for the level of SJF-I (Bonilla-Salomón, et al., 2016). Older localities 200 m down the sequence SJF-II and SJF-III yield ages of approximately 42 Ma corresponding to the Upper Lutetian (MP14; Bonilla-Salomón et al., 2016; Busquets et al., 1992; Badiola et al., 2009).

5.1.3 | Correlation with the GPTS

The integration of the LCM and the above biostratigraphic constraints allows a revised correlation to be put forward with the GPTS (Figure 6) that challenges earlier interpretations (Burbank et al., 1992; Vergés et al., 1998; Garcés et al., 2020).

Biostratigraphic information constrains the age range of the CP section from Maastrichtian–Early Danian at its base, based on charophytes, to the Early Eocene at its top, since the conformably overlying marine Sagnari Formation includes Early Eocene larger foraminifera. During the Danian to the Early Eocene several normal polarity chrons occur (C29n, C28n, C27n, C26n and C25n), which should be recorded in the CP and BA sections since the sampling resolution is high (one sample every 3 m). However, the Coll de Pal section shows just one single reversed magnetozone (R1). A possible explication is that normal polarity chrons are significantly shorter than the reverse ones during the Palaeocene and, in a context of very low sedimentation rates, the short normal polarity intervals were overprinted by the dominantly reverse polarity. For this to happen, the magnetisation lock-in depth should be larger than the thickness of the magnetozones. It is, however, unlikely that chron C29n and C28n are overprinted by dominant reverse polarity as they last almost a million years. On the other hand, a sedimentary hiatus comprising the whole of the Danian and Selandian until the top of chron C25n cannot be excluded. Therefore, two possible scenarios will be considered: (a) the whole period between late-Maastrichtian to the top of chron C25n (57.1 Ma) marks a period of non-deposition and sedimentary bypass in the Ripoll Syncline or (b) deposition occurs after chron C28n (63.5 Ma) during the Palaeocene after a hiatus comprising the Early Danian. (Figures 7 and 8).

In the BA section, the Cadí–Sagnari formations encompass the SBZ5 to SBZ9 biozones suggesting an early Eocene (Ilerdian) age for those deposits. The normal magnetozone N1 observed in the upper part of the Cadí Formation is therefore interpreted as chron C24n. The

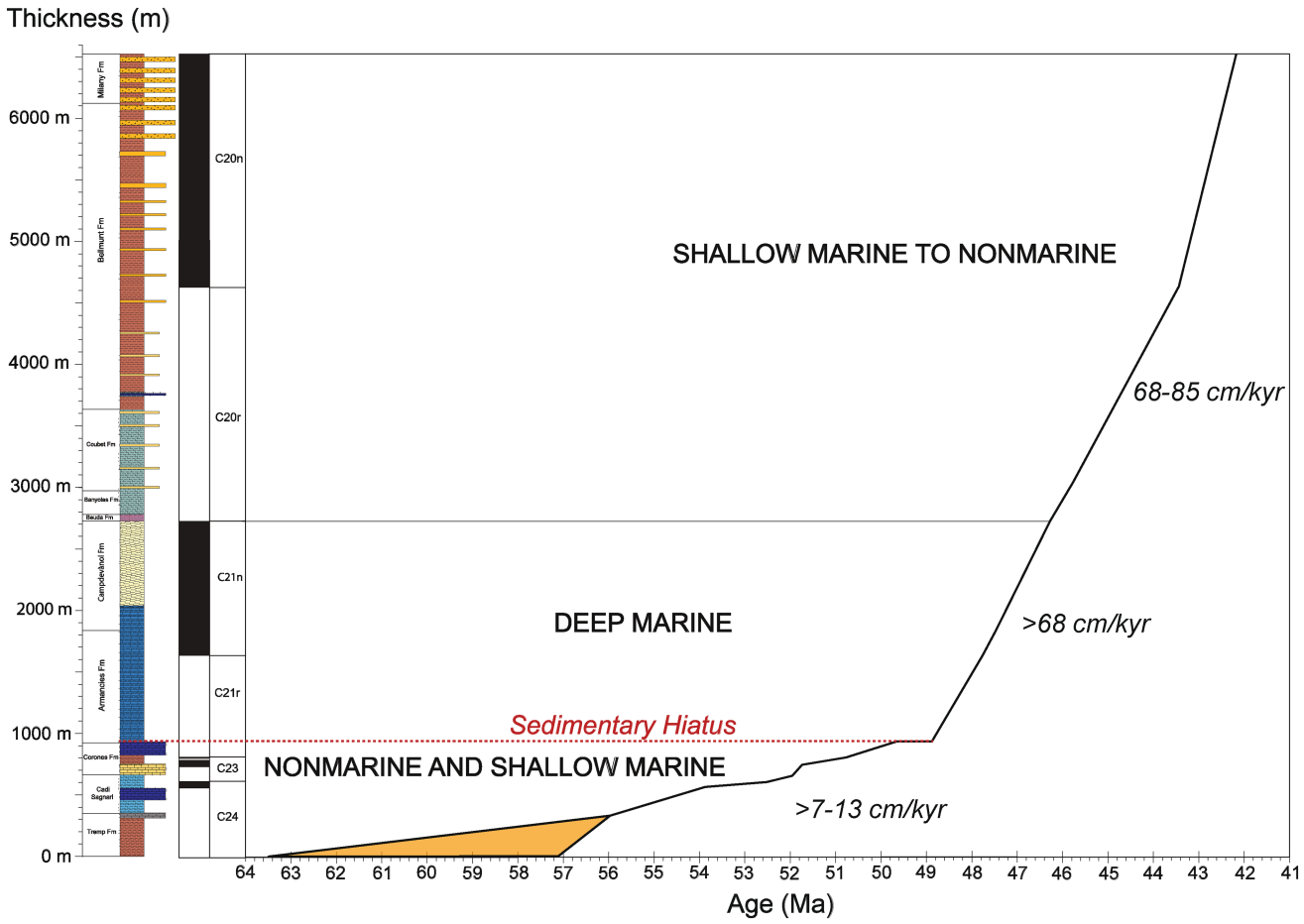

FIGURE 7 Composite magnetostratigraphy and sedimentation trends of the Ripoll Syncline section. Notice the two well-defined sections with different sedimentation rates. Two scenarios (a and b) related to the uncertainty in the age of the base of the section have been considered (in orange).

short reversed subchrons within C24n were not recorded in the magnetostratigraphic section probably because of insufficient sampling resolution, low sedimentation rates and occurrence of unsuitable lithologies such as grainstones, in the Cadí Formation. The series of magnetozones N2, R3 and N3 at the base of the Corones Formation match well with chron C23n (C23n.1n, C23n.1r and C23n.2n) coinciding with the occurrence of SBZ10 biozone at this stratigraphic level. The reverse magnetozone R4, present in the BA and GO sections includes SBZ13 fauna in its upper part. A correlation of R4 to C21r instead of C22r best agrees with the calibration of the SBZ13 elsewhere in the Pyrenean region (Molina et al., 2011), which would imply that chron C22n is not recorded in the composite section presented here, and that R4 should partly correspond to C22r and C21r. The absence of C22n implies a stratigraphic gap, here interpreted as a stratigraphic hiatus. This hiatus has been deduced to be at the sharp basal contact of the carbonate slope Armancies Formation, just atop of the shallow marine carbonate platform Corones Formation Above this interval, a series of mass-transport deposits yield reworked larger foraminifera assemblages representatives of biozones SBZ11,12 and 13. The hiatus at the base of the Armancies Formation, is thus interpreted here as being the result of the destabilisation and collapse of the adjacent carbonate platform as described in other Eocene sections from the Pyrenean foreland basin (Barnolas, 1992; Barnolas & Teixell, 1994; Barnolas et al., 1982, 2019; Payros et al., 1999) and occurring at the transition from carbonate platform to slope deposits. The overlying magnetozones N4, R5 and N5 are correlated with chrons C21n, C20r and C20n, in agreement with the Lutetian age (SBZ13) of larger foraminifera assemblages described in the Campdevànol and Coubet formations.

These correlations result in an age of the topmost deposits corresponding to the top of chron C20n (42.2 Ma).

According to this correlation, the boundaries of the Campdevànol and younger formations are significantly diachronous in a north–south transect, indicating a clear southwards progradation of the clastic system. The vergence of slump folds in the Campdevànol Formation shows a southwards palaeoslope, consistent with a northerly location of the hinterland and the proximal parts of the sedimentary system. On the northern flank of the

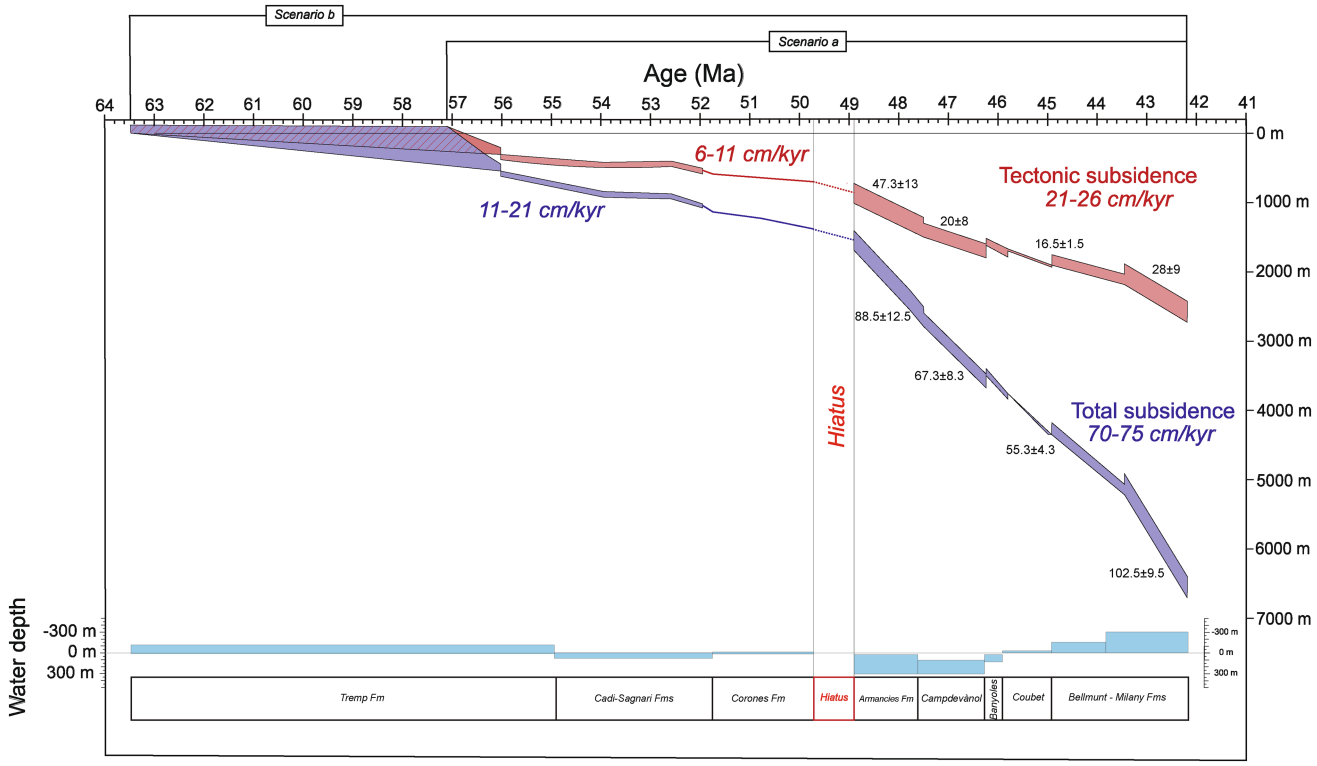

FIGURE 8 Subsidence evolution of the composite Ripoll Syncline section including correlation to lithostratigrapghic units and their palaeobathimetric values. Tectonic and total subsidence show two well-defined episodes (before and after the hiatus at 49 Ma). Two scenarios (a and b) related to the uncertainty in the age of the base of the section have been considered. Total and tectonic subsidence rates (in blue and red respectively) have been calculated considering the palaeobathymetric (shallowing or deepening) trends of each episode or unit.

Ripoll Syncline (PL section), the fluvio-deltaic Banyoles, Coubet and lower Bellmunt formations, which deposited during chron C20r, were contemporaneous with deposition of the Campdevànol turbidites in the southern flank, as previously indicated by Ramos et al. (2002).

5.2 | Biostratigraphic implications

The proposed correlation is the one that best agrees with the existing calibration of the larger foraminifera SBZ scheme of the Early to Middle Eocene (Molina et al., 2011; Rodríguez-Pintó et al., 2012, 2022; Mochales et al., 2012; Silva-Casal et al., 2021). No inconsistencies are observed between correlation of the Cadi–Sagnari and Corones formations and the calibrated ages of the Early Eocene SBZ units. Worth noting is the absence of fossil localities yielding SBZ11 and SBZ12 assemblages other than reworked from shallower platform environments and mixed with younger SBZ13 species, thus suggesting slope environments with minor deposition and dominance of erosion and/or bypass of sediments. The occurrence of a hiatus in the Corones/Armancies transition is claimed to explain the lack of record of chron C22n.

A noticeable disagreement relies on the precise calibration of the SBZ13 age range, that in the Ripoll Syncline section extends from mid-chron C21r to top C20r. The widely accepted correlation of the SBZ12/SBZ13 boundary with the Ypresian/Lutetian boundary (at mid-chron C21r) agrees with the results presented here, but the SBZ13/SBZ14 boundary set in the lower part of C20r in the Gorrondatxe (Molina et al., 2011) and Isuela (Rodríguez-Pintó et al., 2012) sections disagrees with the findings of SBZ13 occurring at the very top C20r (Figure 6).

An outstanding issue from a chronostratigraphic viewpoint arises from the correlation of the magnetozone N5 in the Bellmunt Formation with chron C20n, and the diverging age constraints derived from marine and continental biostratigraphy. As stated above, this correlation challenges the upper limit of the SBZ13, which is found at an older age elsewhere in the Pyrenees. Remarkably, beds included in this same magnetozone N5 host mammal fossils, which yielded a Late Lutetian to Early Bartonian (MP15) age, according to the current calibration of the European MP zonation. Thus, the proposed correlation does not strictly meet the biostratigraphic tiepoints, being too young for the SBZ scheme and too old for the MP zonation. Particularly challenging is the age close to 43 Ma

(Late Lutetian, within chron C20n) given in this study to the mammal site SJF-I, while current biochronological arguments point to a 3 Myr younger age in the early Bartonian (MP15; Bonilla-Salomón et al., 2016; Busquets et al., 1992; Badiola et al., 2009).

Discussing the causes of such conflicting results is beyond the scope of this work. Further studies will be needed to assess the biogeographic aspects and chronostratigraphic significance of some fossil species and their contribution to both marine and continental chronostratigraphic scales.

5.3 | Geohistory

5.3.1 | Stratigraphic cycles

The whole analysed Palaeogene Ripoll Syncline section shows a general transgressive–regressive trend. It starts with non-marine and shallow marine sediments (Palaeocene to Middle Cuisian), followed by deep marine (Late Cuisian to Early Lutetian) which finally evolve to shallow marine and non-marine strata (Early to Middle Lutetian). However, this succession can be subdivided into three major transgressive–regressive cycles (Figure 4): The first depositional cycle is marked by transgressive–regressive marine Late Cretaceous units of the Areny sequence bounded atop by a regional unconformity below Palaeocene strata. The second depositional cycle is bounded at its base by the above mentioned Cretaceous–Palaeocene unconformity and includes red Garumnian facies evolving from alluvial to lacustrine (Van Eeckhout et al., 1991), the Cadí and Sagnari formations representing the deeper marine strata and finally the regressive lower Corones Formation culminating in non-marine red beds. The third cycle starts with the transgressive shallow marine limestones of the uppermost Corones Formation, overlain by the carbonate slope deposits of the Armancies Formation. The regressive part of the cycle consists of a thick prograding clastic wedge embracing the Campdevànol, Banyoles, Coubet, Bellmunt and Milany formations, grading from deep marine to proximal alluvial environments.

Contrary to what is shown in Vergés et al. (1998), where the Beuda evaporites mark the boundary between their sequences 2 and 3, it is not thought that the evaporites that crop out in the studied GO, LP and SJF sections are of key stratigraphic significance. They form discontinuous bodies at the top of the Campdevànol Formation scattered at different stratigraphic positions across the flanks of the syncline (Figures 2, 3 and 4). Some of these could be primary evaporitic deposits, and others represent olistoliths of Triassic evaporites eroded from the northern upper cover thrust sheet and brought to the basin by mass-gravity processes (Puigdefàbregas et al., 1986). Southwards, the Beuda (and Serrat) Formation forms a large evaporitic unit interpreted as the lateral and proximal equivalent of the Campdevànol Formation (Carrillo et al., 2014, 2017) and may have been caused by basin restriction and isolation from oceanic masses by the emplacement of the Pedraforca Nappe conjugated with a global sea-level fall (Puigdefàbregas et al., 1986).

The regressive part of the third cycle involves shallow water and transitional facies, which are prone to respond to higher-frequency oscillations. Several transgressive and regressive trends are observed in the Coubet, Bellmunt and Milany formations, which probably resulted from cyclicity of higher order than the ones defined previously.

The defined cycles have been interpreted from the studied vertical section. Their boundaries and major surfaces as maximum flooding surfaces probably do not have chronostratigraphic significance. One of the main key surfaces, related to the change from transgressive to regressive in the second cycle must be in the upper Armancies or lower Campdevànol formations, correlated to the deepest bathymetry. This change from carbonate slope (related to the southern margin platforms) to deep marine clastics is probably not a timeline but a heterochronous contact since southern carbonate platforms are time equivalent to clastics with a northern provenance (Vergés et al., 1998; Garcés et al., 2020) as observed in other south Pyrenean sub-basins (Vinyoles et al., 2021). As predictable from the asymmetrical distribution of depozones and the general evolution of foreland systems, the overall regressive trends in the northern clastic margin (Corones, Campdevànol-Banyoles-Coubet-Bellmunt) were coeval with the transgressive trends in the southern platforms (Cadí, Penya, Tavertet), making it unfeasible to trace chronostratigraphic limits based solely on the sequential arrangement.

5.3.2 | Sedimentation and subsidence evolution of the Ripoll Syncline

From the correlation of the LCM with the GPTS an estimation of compacted sedimentation rates can be obtained (Figure 7). A large uncertainty remains in the rates assigned to the Tremp Formation given the uncertainty in the correlation of the base of the section with the GPTS, as discussed above. Added to this, the duration of the hiatus at the base of the Armàncies Formation cannot be accurately estimated, and a minimum hiatus equivalent to the duration of the missing chron C22r is assigned. This means that the rates obtained for the bounding intervals are minimum values.

The average sedimentation rate of the composite succession is close to 50 cm/kyr standing within the average values of 10–100 cm/kyr for sedimentation rates in foreland basins (Einsele, 2000). The sedimentation trend shows two segments with distinct slopes separated by a hiatus. The first one, comprising the Tremp, Cadí, Sagnari and Corones formations yields values of 7–13 cm/kyr, whereas the second one, comprising Armàncies, Campdevànol, Banyoles, Beuda and Bellmunt formations yields much higher values, about 68–85 cm/kyr. These sedimentation rates are comparable to those obtained by Vinyoles et al. (2021) in the Jaca Basin, a contemporary south Pyrenean sub-basin in the Western Pyrenees (7 cm/kyr for the shallow marine platforms in the southern Jaca forebulge and 53 cm/kyr for the deep marine to continental shallowing upward succession from foredeep to wedge-top setting). Also, the sedimentation rates observed in each sedimentary environment reproduce a pattern similar to the Jaca Basin: Deep marine (68 cm/kyr in Ripoll, 54 cm/kyr in Jaca), deltaic progradation (68–85 cm/kyr and 71 cm/kyr respectively).

A thorough analysis of the subsidence was previously performed by Vergés et al. (1998) along a north–south transect in the Eastern South Pyrenean foreland basin. In this paper, the subsidence evolution is reviewed in the light of a revised chronostratigraphic framework (Figure 8). Given the age uncertainty of the base of the studied succession, two scenarios were considered for the analysis, taking its youngest (scenario a) and the oldest (scenario b) possible age. Subsidence rates were calculated for the duration of each chron considering those values within the admissible palaeobathymetric range that yielded the smoothest trends honouring their deepening or shallowing upwards trend. The resulting subsidence curve shows two well-defined episodes. First, a Palaeocene to Early Eocene interval (63.5 Ma/57.1–49.7 Ma) with low total (11–21 cm/kyr) and tectonic (6–11 cm/kyr) subsidence rates. Second, an early to middle Eocene interval (48.9–42.2 Ma), characterised by higher total (70–75 cm/kyr) and tectonic (21–26 cm/kyr) subsidence rates. In this second interval, after the sharp initial increase of subsidence, a smooth decreasing to increasing trend (from 89 to 55 to 103 cm/kyr in total subsidence, and from 47 to 17 to 28 cm/kyr in tectonic subsidence) can be observed.

The described trends in both subsidence and sedimentation in the Cadí Nappe can be linked with the predictable development of depozones in foreland systems (DeCelles & Giles, 1996), evolving from a distal foreland depozone (forebulge depozone?) with low subsidence and low sedimentation rates in a non-marine to shallow marine environment to a highly subsiding foredeep depozone marked with expanded deep marine sedimentation evolving into shallow marine and even continental environments. The shallowing trend of the foredeep sedimentation is interpreted as related to the increasing sediment flux derived from the growing catchment area on the emerging orogen. This is a typical evolution in pro-foreland basin systems, where the load-related regional flexural subsidence migrates basinwards and the clastics derived from the hinterland denudation progressively fill the basin (DeCelles & Giles, 1996; Vinyoles et al., 2021).

The smooth sigmoidal shape of the subsidence curves typical of foreland basins is not observed here. First, the transition from low subsidence values in the distal foreland depozones to high rates in the foredeep is not gradual but abrupt. This is probably due to the presence of hiatuses that disrupted the record during the transition into slope sedimentation. Following the peak stage of subsidence during deposition of the Armancies Formation, the progressive reduction of the tectonic subsidence would reflect the relaxation of the tectonic loading. Noticeably, the total subsidence during this time was kept at high rates favoured by the sediment load of the rapidly filling trough. Second, a significant increase of subsidence is experienced during the deposition of the top Milany Formation, which is particularly remarkable since it happened at times of the emplacement of the Cadí Nappe, when the region was incorporated into the wedge-top depozone. This subsidence increase could be related to the renewed tectonic load caused by the breakback reactivation of the Lower Pedraforca Thrusts and the coeval growth of the Freser antiformal stack (Martínez et al., 1988). Added to this, a local influence is possibly caused by the sampling strategy of the studied section progressing upwards from the (condensed) limbs to the (expanded) hinge of the growth syncline. Lastly, the emergence of the Vallfogona Thrust could have impacted the sediment routing, blocking the south-directed transverse sediment transport and possibly creating a short-lived intramontane depocentre with an elevated base level and aggradation of alluvial units.

5.3.3 | Tectono-sedimentary evolution

As indicated by Puigdefbregas, et al. (1986), Martínez et al. (1988) and Vergés (1993) among others, the evolution of the eastern South Pyrenean foreland basin is closely related to the tectonic evolution of the area and the piggy-back thrust sequence. The evolution presented herein (Figure 9) is based in these previous works and includes new sedimentologic and chronostratigraphic data.

The northern margin of the Iberian plate underwent tectonic inversion and orogenic growth during the Campanian–Maastrichtian (Figure 9A). Slow subsidence in the still not differentiated Cadí Nappe led to the accumulation of a condensed marine to lagoonal sedimentary

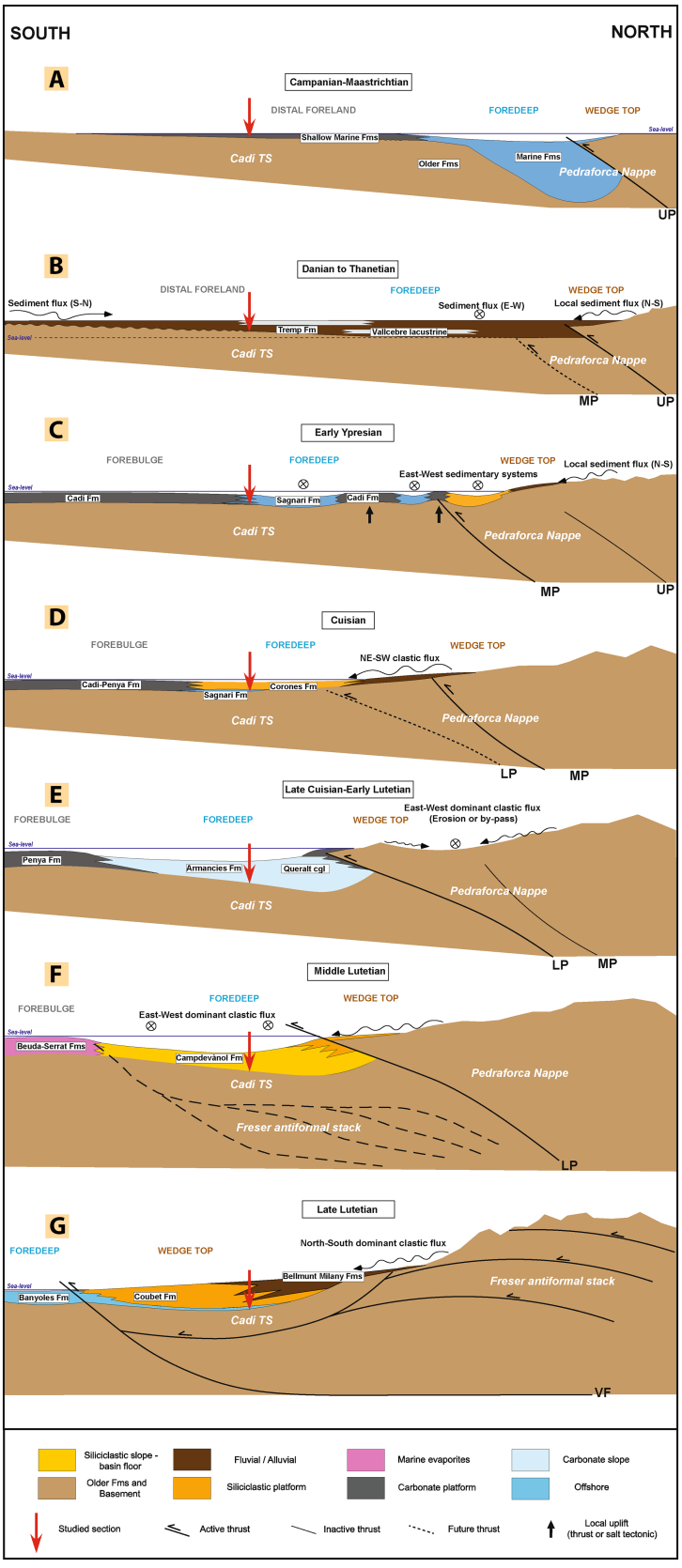

FIGURE 9 Summary evolution of the landscape, sedimentary environments and depozones along a N-S cross-section of the Eastern South Pyrenean foreland in seven time steps. Note the southwards displacement of the deformation front and the corresponding progressive displacement of the deformation front and associated foreland flexure that forces the southward movement of the depozones. No vertical or horizontal scale. LP, Lower Pedraforca Thrust; MP, Middle Pedraforca Thrust; UP, Upper Pedraforca Thrust; VF, Vallfogona Thrust.

succession, unconformably over Triassic and basement units and overlain by unconformable red Garumnian facies (Oms et al., 2016). Northwards, in the domain of the still undifferentiated Lower and Middle Pedraforca nappes, the sedimentation was continuous with increasingly thicker units and deeper environments towards the north (Oms et al., 2016; Vergés et al., 1994), marking the development of the foredeep related to the emplacement

of the Upper Pedraforca Nappe (Martínez et al., 1988; Vergés et al., 1995). The correlative wedge-top depozone was placed in the domain of the Upper Pedraforca, characterised by a reduced thickness of syn-orogenic Late Cretaceous sediments (Cruset et al., 2021).

It is probably that the hiatus at the base of the Garumnian facies in the CP section, ranging from Late Cretaceous to possibly Late Thanetian, was coeval to the emplacement of the Upper Pedraforca Nappe (Figure 9B). At this initial stage the Cadí Nappe was in a distal foreland depozone position. The onlap of the Tremp Formation onto the Hercynian basement towards the southern margin marks the sense of migration of the flexural deformation (Vergés 1993; Bello et al., 2008; Vergés et al., 1994). Towards the north, red Garumnian units partially fossilise the Upper Pedraforca Thrust (Vergés, 1993), giving a Palaeocene age for the final stages of its emplacement. The tectonic subsidence related to the emplacement of the Upper Pedraforca cover Thrust Sheet was relatively minor, leading to low rates of sedimentation of the Garumnian facies, from 7 to 13 cm/kyr in the Cadí nappe (Figure 7) and 7 cm/kyr in the Vallcebre Syncline of the Lower Pedraforca Nappe (Oms et al., 2016).

The Garumnian facies were followed by deposition of marine sediments (Cadí and Sagnari formations) and siliciclastic platform deposits from a northern source (Corones Formation) until 49.7 Ma (base of chron C22n), marking a transgressive–regressive period of low sedimentation rates (Figure 9C,D). The Early Eocene transgressive trend could be attributed to the conjugation of increased sea level (Ilerdian transgression) and/or the incipient flexural response to orogenic growth. A condensed and/or discontinuous sedimentation during the deposition of the Cadí and lower Corones formations can be inferred from the incomplete record of chrons C24n and C23n in the BA section (Figure 6). This fits with a context of forebulge (Cadí Formation) or distal foredeep (Sagnari Formation) development in the Cadí Nappe relative to the emplacement of the Middle Pedraforca. The outer ramp marls (Sagnari Formation), with deltaic incursions reveals that terrigenous sediments were fed from a north-eastern source since Ilerdian times (Vergés et al., 1998; Garcés et al., 2020). Platform carbonates (Cadí Formation) developed extensively towards the southern margin of the basin (Cadí and Ebro basins) but also to the north, in the Lower and Middle Pedraforca nappes. Effectively there is a series of carbonate platform outcrops on the Lower (Queralt, Espinalbet, Puig Cubell) and Middle Pedraforca nappes (Malanyeu; Mató et al., 1994; Vergés et al., 1994; Martínez et al., 2020). The presence of shallow marine clastic units is also noteworthy, and these are attributed to the same Early Eocene age in the Middle Pedraforca Nappe (Peguera Syncline; Martínez et al., 1988). These Early Eocene clastic sediments represent shallow marine deposition in the hangingwall of the Middle Pedraforca active thrust in a wedge-top position. The carbonates initially both in the footwall and hangingwall of the Middle Pedraforca would represent relatively clastic-free deposition atop positive growth structures (anticlines), whereas clastic systems could be confined (Martínez et al., 1988) and routed along synclines. This situation is typical of a wedge-top and can be interpreted as resulting from the growth of the hangingwall anticline simultaneously with the emplacement of the Middle Pedraforca, favouring the development of clastic-free carbonate platforms that grade north to sandy facies derived from the Pyrenean landforms and south to deeper offshore muds (Sagnari Formation) in the foredeep. However, this situation of localised platforms grading north and south to deeper clastic facies (offshore mudstones) is also found in the foredeep (e.g. Queralt carbonate platforms). This could be associated with a topography of submarine highs and lows related to the growth of evaporite-cored anticlines in the foredeep region linked to tectonic load-driven salt migration coeval with emplacement of the Middle Pedraforca. A similar situation has been described in the South-Central Pyrenees (Holl & Anastasio, 1993; Santolaria et al., 2016; Soto et al., 2002).

The top of the Corones Formation is marked by a transgressive event evidenced by the vertical evolution from non-marine to shallow marine carbonate and mixed platform. This trend is followed by the Corones/Armancies boundary (48.9 Ma, base of chron C21r) with the shifting of the sedimentary environment to distal ramp and carbonate slope (Giménez, 1989), indicating a sudden deepening of the basin floor and a noticeable increase of tectonic subsidence (Figure 8). This was caused by the combination of the local tectonic load of the Lower Pedraforca (Puigdefàbregas et al., 1986; Vergés et al., 1998), and the consequent forelandwards migration of the lithospheric flexure of the Iberian plate under the overriding European plate. The Corones/Armàncies transition, thus, represents the transition from distal foreland depozones (slowly subsiding non-marine and shallow marine succession) to foredeep (highly subsiding slope to deep marine succession).

It was a period of important reorganisation of the basin profile (Figure 9E), giving rise to a narrow and elongated trough parallel to the orogenic front, with its southern margin grading to the carbonate platforms of the Penya Formation. This important change has been interpreted as related to the shift of the deformation front from the Middle Pedraforca to the Lower Pedraforca Nappe. A ≥800 kyr hiatus, equivalent to the age range of chron C22n (from 49.7 to 48.9 Ma), is interpreted as resulting from destabilisation and collapse of the adjacent carbonate

platforms, evidenced by the occurrence of slope breccias of resedimented platform carbonates interbedded in the Armancies Formation. An interesting feature of the initial stage of a clear foredeep in the Cadí Nappe is that the Armancies Formation was devoid of major siliciclastic inputs.

This could reflect the early submarine emplacement of the Lower Pedraforca and, linked to it, the formation of a ridge that temporarily blocked the transport of clastic sediments from the Pedraforca to the Cadi Nappe, and routed the sediment flux from emerged areas onto the Lower Pedraforca Nappe to westerly sinks. This submarine high in the wedge-top depozone would act as the substratum of carbonate platforms situated to the northern edge of the trough, and these as the source of the slope breccia deposits of the lower Armancies Formation (Tosquella, 1995). In support of the presence of these northern carbonate platforms, the Cuisian-Lutetian conglomerates of Queralt, in the Lower Pedraforca Nappe (Vergés et al., 1994), bear platform-derived clasts of unambiguous northern provenance (Ullastre et al., 1990; Gilham & Bristow, 1998). Foraminiferal assemblages in the Queralt conglomerates support a correlation with the upper Armancies Formation in the Cadí Nappe, thus indicating that these are the proximal equivalents of the slope turbiditic sediments filling the foredeep (Solé Sugrañes & Clavell, 1973).

At *ca* 47.5 Ma, the transition into the turbidites of the Campdevànol Formation marks the entry of siliciclastic sediments, related to the rapid emersion of the orogenic wedge and the end of the tectonic-related clastic starvation in the basin (Figure 9F). Palaeocurrent data indicate a progradation of the clastic wedge to the west-south-west, parallel to the basin axis, followed by a gradual vertical transition into shallow marine (Banyoles and Coubet formations; Puigdefàbregas, 1986; Vergés et al., 1994) and then fluvial facies (Bellmunt Formation), while keeping high rates of sedimentation (Figure 7). This indicates that the filling of the foredeep occurred while subsidence was high, allowing the Ripoll Trough to act as an efficient sink for sediment flux of north-eastern provenance. This initial foredeep period (including the Armàncies Formation) represents the underfilled accommodation stage of the foreland basin (Vergés et al., 1998) and coincides with the time of highest rates of tectonic shortening (>4 mm/year) and rapid thrust-front advance (Vergés et al., 1995). Underfilled accommodation conditions were maintained up to the middle Lutetian during the deposition of the Campdevànol siliciclastic turbidites, until complete filling of the marine basin by progradation of the fluvio-deltaic system still in the foredeep depozone. The correlation proposed in this study evidences the overall cratonwards progradation of the clastic wedge (Campdevànol, Banyoles, Coubet, Bellmunt and Milany formations) typical of foreland systems.

At the front of the Lower Pedraforca Thrust a fold-propagation fold, the Vilada Anticline, developed synchronously with deposition of the Coubet and lower Bellmunt formations (Martínez et al., 1988), providing an age for the thrust emplacement (fossilisation) of approximately 43.5 Ma. Alluvial sediments overlying the Bellmunt Formation developed unconformities that indicate the synchronous growth of the Ripoll Syncline. This syncline is related to the growth of the Freser Antiform to the north, and the tectonic transport of the Cadí Nappe onto the footwall ramp of the Vallfogona Thrust (Martínez et al., 1988). The onset of the Vallfogona Thrust and growth of the Ripoll Syncline marks therefore the transition of the Cadí Nappe into the wedge-top stage at an age close to 43.5 Ma (within chron C20n; Figure 9G). Palaeocurrent data from the SJF and PL sections contributed to the palaeogeographical reconstruction of the late filling stage of the Ripoll Syncline (Ramos et al., 2002). In the upper part of the sedimentary succession, the transition from the Bellmunt to the Milany formation reveals a shift in the sediment palaeocurrent, from an axial transport, directed to the west, to a transverse system with palaeocurrents directed to the south. This change points to the Ripoll Syncline overfill and the initiation of direct sediment bypass towards the Ebro foreland, and the filling of the foredeep now located on the footwall of the Vallfogona Thrust. There, the transition from platform carbonates of the Tavertet Formation to the marls of the Coll de Malla Formation (Serra-Kiel et al., 2003) would mark the shift from forebulge to foredeep in the Eastern Ebro Basin (Vergés et al., 1998) during the Late Lutetian.

As summary, the Palaeocene red Garumnian in the Ripoll Syncline correlates to a distal foreland depozone situation coeval with the last stages of emplacement of the Upper Pedraforca Thrust Sheet. Its basal unconformity above Late Cretaceous strata is a product of uplifting in this scenario.

The Early Eocene interval (Late Palaeocene to Middle Cuisian) comprising the Cadí, Sagnari and prograding Corones formations is related to the emplacement of the Middle Pedraforca Thrust, which did not generate high subsidence and relief. Coeval with this thrust, shallow deformation resulting in shallow marine highs and lows developed both in the hangingwall and footwall. This thrust activity is translated into a transgressive–regressive cycle with low sedimentation and subsidence rates and shallow marine to non-marine sedimentation attributed to a distal foreland depozone to distal foredeep context.

The Early to Middle Eocene interval (Late Cuisian to Early Lutetian), comprising the transgressive Corones to Bellmunt formations, shows again a general transgressive

to regressive trend. This period would be related to a new thrust or set of thrusts (Lower Pedraforca) following the in-sequence evolution of the thrust system. This implies an important increase in subsidence rates and an evolution from the initial distal foreland depozones situation (Corones Formation) to a foredeep (Armàncies to Bellmunt formations), which is progressively filled by clastics due to the relief generated during this period. After the initial increase, subsidence rates show a progressive decrease probably related to a decline of tectonic activity.

The Middle Lutetian interval, comprising the Bellmunt and Milany formations, shows an increase in subsidence rates but associated with non-marine sediments having a general regressive–progradational trend. This interval corresponds to the initial stages of the Vallfogona Thrust emplacement which individualised the Cadí Nappe, the breakback reactivation of the Lower Pedraforca Thrusts and the growth of the Freser antiformal stack producing both, an increase of the loading favouring renewed subsidence and generation of reliefs feeding the basin with coarse grained clastics.

5.3.4 | Sediment provenance in the Ripoll Syncline

According to Odlum et al. (2019) and Gómez-Gras et al. (2016), most of the Garumnian sediments of the CP section (*Sample 16-RB-003*) were sourced from Palaeozoic massifs to the east and south-east (Montseny Massif and Corsica-Sardinia Block), with minor input from the nascent Pyrenean chain. Therefore, according to the new age model southern sources possibly prevailed until Late Thanetian times in the Cadí Nappe. It is during deposition of the Sagnari Formation when a dominant Pyrenean source of sediments was established, a change that is interpreted as marking the emergence of the orogen (Odlum et al., 2019). These authors further interpret the coeval transition into marine conditions as resulting from flexural subsidence linked to orogenic wedge growth.

However, subsidence analysis shows that after a hiatus spanning the Early Danian to, possibly, Thanetian, slow tectonic subsidence initiated (63.5 and 57.1 Ma) and alluvial sediments sourced from the south-southeast accumulated on the Cadí Nappe. Sediment provenance switched to a northern source with no significant change in the subsidence trend, but coeval with the transition to marine conditions in the basin (Sagnari Formation, 55.5 Ma). Thus, it is unclear that the change of sediment source was caused by tectonics. A change in the palaeogeography driven by a rising sea level, with a marine domain extending between the Iberian and Pyrenean land masses (the Ilerdian transgression), could have reorganised the sediment routing, limiting the sediment flux from the Iberian margin towards the Pyrenean foredeep. These conditions allowed an increased proportion of sediment input from the emergent Pyrenees during deposition of the Sagnari Formation without the need to invoke further uplift.

6 | CONCLUSIONS

New magnetostratigraphic sections studied in the Ripoll Syncline (Eastern Pyrenees), spanning Palaeocene to Middle Eocene times are integrated with new charophyte biostratigraphy and earlier magnetostratigraphic and marine and continental biostratigraphic data to produce a revised chronostratigraphy of the Palaeogene sedimentary sequences of the Cadí Nappe.

The new chronostratigraphic framework has enabled a revision of the timing of thrusting, sedimentation and subsidence through the evolution of the South Pyrenean foreland. The identification of the different depozones of the foreland system and their distribution through time reveals a stepwise cratonwards migration of the foreland as the nappes were emplaced in a piggy-back thrust sequence.

The sea-level rise at 55.5 Ma (Ilerdian transgression) contributed to a reorganisation the sediment routing by limiting the sediment flux from the southern Iberian margin (Tremp Formation) in favouring the inputs from the emerging Pyrenees into the nascent foredeep.

The transition from distal foreland depozones to a foredeep situation is marked by the presence of a hiatus. This is interpreted as related to the development of a non-depositional slope between the carbonate platform and slope after the drowning of the platform due to a subsidence induced relative sea-level rise. The submarine growth of structures related to the initial emplacement of the Middle Pedraforca Nappe or to salt-related processes possibly conditioned the sediment routing in an early stage, blocking the transverse southwards transport to the foredeep and favouring an axial westward transport. In a later stage, the deep and rapidly subsiding Ripoll sedimentary trough acted as an effective sink for turbiditic fans (Campdevànol Formation) sourced from the emergent orogen. Sediments corresponding to the youngest wedge-top setting were preserved in the core of the growing Ripoll Syncline (upper Bellmunt and Milany formations).

Noteworthy in the evolution of the Ripoll trough was the filling rate, with the accumulation of as much as 5500 m of sedimentary thickness in less than 7 Myr, leading to a transition from underfilled to overfilled accommodation stage in the Middle Eocene, a much faster pace than that recorded in the western South Pyrenean region (Jaca Basin), where the formation of the foredeep

was approximately synchronous, but the overfilling of the trough was accomplished in much younger times, during the Oligocene.

Similarly, to the Jaca Basin, remarkably high sedimentation rates in the wedge-top depozone were maintained as the regional subsidence related to the emplacement of basement units in the hinterland counterbalanced the local uplift of the Cadí Nappe overriding on the Vallfogona Thrust.

ACKNOWLEDGEMENTS

This is a contribution of the Marie Skłodowska-Curie Innovative Training Networks from the European Union (H2020-MSCA-ITN-2019) Signal Propagation in Source to Sink for the Future of earth Resources and Energies (S2S-Future). Partially funded with Spanish project PID2019-106440GB-C21 (Ministerio de Ciencia, Innovación y Universidades).

DATA AVAILABILITY STATEMENT

The data that support the findings of this study are available from the corresponding author, [PJ], upon reasonable request.

ORCID

Philémon Juvany https://orcid.org/0000-0002-2869-1064
Miguel Lopez-Blanco https://orcid.org/0000-0001-6763-0355
Carles Martín Closas https://orcid.org/0000-0003-4349-738X

REFERENCES

Badiola, A., Checa, L., Cuesta, M.A., Quer, R., Hooker, J.J. & Astibia, H. (2009) The role of new Iberian finds in understanding European Eocene mammalian paleobiogeography. *Geologica Acta*, 7, 243–258. https://doi.org/10.1344/105.000000281

Barnolas, A., Ríos Aragües, L., Lanaja, J.M. & Frutos, E. (1982) *Hoja 178 (Broto) Mapa Geológico de España E. 1:50.000. Serie MAGNA*. Madrid: IGME.

Barnolas, A. (1992) Evolución sedimentaria de la Cuenca Surpirenaica Oriental durante el Eoceno. *Acta Geologica Hispánica*, 27(1–2), 15–31.

Barnolas, A. & Teixell, A. (1994) Platform sedimentation and collapse in a carbonate-dominated margin of a foreland basin (Jaca basin, Eocene, southern Pyrenees). *Geology*, 22, 1107–1110. https://doi.org/10.1130/0091-7613(1994)022<1107:PSACIA>2.3.CO;2

Barnolas, A., Larrasoaña, J.C., Pujalte, V., Schmitz, B., Sierro, F.J., Mata, M.P., van den Berg, B.C.J., Pérez-Asensio, J.N., Salazar, Á., Salvany, J.M., Ledesma, S., García-Castellanos, D., Civis, J. & Cunha, P. (2019) Alpine Foreland Basins. In: Quesada, C. & Oliveira, J. (Eds.) *The geology of Iberia: a geodynamic approach*. Cham, Switzerland: Springer, pp. 7–59. https://doi.org/10.1007/978-3-030-11190-8_2

Bello, D., López-Blanco, M., Muñoz, J.A., Roca, E., Casas, J.M. & Marzo, M. (2008) Estructura del sistema frontal de cabalgamientos en el Pirineo Oriental: control estratigráfico en la geometría y secuencia de emplazamiento de los cabalgamientos. *Geotemas*, 10, 321–324.

Blair, T.C. & McPherson, J.G. (1994) Alluvial fans and their natural distinction from rivers based on morphology, hydraulic processes, sedimentary processes, and facies assemblages. *Journal of Sedimentary Research*, 64(3a), 450–489. https://doi.org/10.1306/D4267DDE-2B26-11D7-8648000102C1865D

Bonilla-Salomón, I., Minwer-Barakat, R., Vianey-Liaud, M. & Moyà-Solà, S. (2016) Middle Eocene rodents from Sant Jaume de Frontanyà (eastern Pyrenees, northern Spain) and biochronological implications. *Journal of Vertebrate Paleontology*, 36(4), e1121149. https://doi.org/10.1080/02724634.2016.1121149

Burbank, D.W., Puigdefàbregas, C. & Muñoz, J.A. (1992) The chronology of the Eocene tectonic and stratigraphic development of the eastern Pyrenean foreland basin, northeast Spain. *Geological Society of America Bulletin*, 104, 1101–1120. https://doi.org/10.1130/0016-7606(1992)104<1101:TCOTET>2.3.CO;2

Busquets, P., Ramos Guerrero, E., Moya, S., Agusti, J., Colombo, F., Checa, L. & Kohler, M. (1992) La Formación de Bellmunt (Unidad del Cadi, Pirineo Oriental); aportaciones bioestratigráficas de los sistemas lacustres y palustres asociados. *Acta Geologica Hispánica*, 27, 109–116.

Carrillo, E., Rosell, L. & Ortí, F. (2014) Multiepisodic evaporite sedimentation as an indicator of palaeogeographical evolution in foreland basins (South-eastern Pyrenean basin, Early-Middle Eocene). *Sedimentology*, 61, 2086–2112. https://doi.org/10.1111/sed.12140

Carrillo, E., Koyi, H.A. & Nilfouroushan, F. (2017) Structural significance of an evaporite formation with lateral stratigraphic heterogeneities (Southeastern Pyrenean Basin, NE Spain). *Marine and Petroleum Geology*, 86, 1310–1326. https://doi.org/10.1016/j.marpetgeo.2017.07.024

Castel, M. (1969) Sur les charophytes de l'Éocène inférieur de Provence. *Comptes Rendus Académie des Sciences, Paris*, 268, 1589–1592.

Choukroune, P. (1989) The Ecors Pyrenean deep seismic profile reflection data and the overall structure of an orogenic belt. *Tectonics*, 8, 23–39. https://doi.org/10.1029/TC008i001p00023

Comte, B., Sabatier, M., Marandat, B. & Vianey-Liaud, M. (2012) Les Rongeurs de Chery-Chartreuve et Rocourt-Saint-Martin (Est du Bassin de Paris; Aisne, France). Leur place parmi les faunes de l'Éocène Moyen d'Europe. *Palaeovertebrata*, 37, 167–271. https://doi.org/10.18563/pv.37.4-5.167-271

Cruset, D., Vergés, J., Benedicto, A., Gomez-Rivas, E., Cantarero, I., John, C.M. & Travé, A. (2021) Multiple fluid flow events from salt-related rifting to basin inversion (Upper Pedraforca thrust sheet, SE Pyrenees). *Basin Research*, 33, 3102–3136. https://doi.org/10.1111/bre.12596

DeCelles, P.G. & Giles, K.A. (1996) Foreland basin systems. *Basin Research*, 8(2), 105–123. https://doi.org/10.1046/j.1365-2117.1996.01491.x

Domingo, L., López-Martínez, N., Leng, M.J. & Grimes, S.T. (2009) The Paleocene–Eocene thermal maximum record in the organic matter of the Claret and Tendruy continental sections (South-central Pyrenees, Lleida, Spain). *Earth and Planetary Science Letters*, 281(3–4), 226–237. https://doi.org/10.1016/j.epsl.2009.02.025

Einsele, G. (2000) *Sedimentary basins: evolution, facies, and sediment budget*. Berlin, Heidelberg: Springer. https://doi.org/10.1007/978-3-662-04029-4

Feist-Castel, M. (1975) Répartition des charophytes dans le Paléocène et l'Éocène du bassin d'Aix-en-Provence. *Bulletin de la Société Géologique de France*, 17, 88–97. https://doi.org/10.2113/gssgfbull.S7-XVII.1.88

Feist, M. & Colombo, F. (1983) La limite Crétacé-Tertiaire dans le nord-est de l'Espagne, du point de vue des charophytes. *Géologie Méditerranéenne*, 10(3,4), 303–326. https://doi.org/10.3406/geolm.1983.1273

Ford, M., Hemmer, L., Vacherat, A., Gallagher, K. & Christophoul, F. (2016) Retro-wedge foreland basin evolution along the ECORS line, eastern Pyrenees, France. *Journal of the Geological Society*, 173, 419–437. https://doi.org/10.1144/jgs2015-129

Garcés, M., López-Blanco, M., Valero, L., Beamud, E., Muñoz, J.A., Oliva -Urcia, B., Vinyoles, A., Arbués, P., Cabello, P. & Cabrera, L. (2020) Paleogeographic and sedimentary evolution of the south-Pyrenean foreland basin. *Marine and Petroleum Geology*, 113, 104105. https://doi.org/10.1016/j.marpetgeo.2019.104105

Gich, M. (1973) Estudio geológico del Eoceno prepirenacio del Ripollés oriental. *Acta Geologica Hispánica*, VIII(4), 120–124.

Gilham, R.F. & Bristow, C.S. (1998) Facies architecture and geometry of a prograding carbonate ramp during the early stages of foreland basin evolution: lower Eocene sequences, Sierra del Cadí, SE Pyrenees, Spain. *Geological Society, London, Special Publications*, 149(1), 181–203.

Giménez, J. (1989) Els materials deltaic i de plataforma del Cuisià Inferior (Eocè Inferior) de la conca sudpirinenca catalana. Sector Bagà-Pobla de Lillet. MSc Thesis, Universitat de Barcelona.

Giménez-Montsant, J., Calvet, F. & Tucker, M.E. (2002) Silica diagenesis in Eocene shallow-water platform carbonates, southern Pyrenees. *Sedimentology*, 46, 969–984. https://doi.org/10.1046/j.1365-3091.1999.00231.x

Gómez-Gras, D., Roige, M., Fondevilla, V., Oms, O., Boya, S. & Remacha, E. (2016) Provenance constraints on the Tremp Formation paleogeography (southern Pyrenees): Ebro Massif VS Pyrenees sources. *Cretaceous Research*, 57, 414–427. https://doi.org/10.1016/j.cretres.2015.09.010

Gradstein, F.M. & Ogg, J.G. (2020) Chapter 2—The chronostratigraphic scale. In: Gradstein, F.M., Ogg, J.G., Schmitz, M.D. & Ogg, G.M. (Eds.) *The geologic time scale 2020, Vol. 1*. Amsterdam: Elsevier, pp. 21–32.

Grool, A.R., Ford, M., Vergés, J., Huismans, R.S., Christophoul, F. & Dielforder, A. (2018) Insights into the crustal-scale dynamics of a doubly vergent orogen from a quantitative analysis of its forelands: a case study of the eastern Pyrenees. *Tectonics*, 37, 450–476. https://doi.org/10.1002/2017TC004731

Holl, J.E. & Anastasio, D.J. (1993) Paleomagnetically derived folding rates, southern Pyrenees, Spain. *Geology*, 21, 271–274. https://doi.org/10.1130/0091-7613

Martínez, A., Vergés, J. & Muñoz, J.A. (1988) Secuencias de propagación del sistema de cabalgamientos de la terminación oriental del manto del Pedraforca y relación con los conglomerados sinorogénicos. *Acta Geologica Hispánica*, 23, 119–128.

Martínez, A., Losantos, M., Domingo, F., Samsó, J.M., Saula, E., Soriano, C., Schöllhorn, E., Gisbert, J., Casas, J.M. & Caus, E. (2020) *Hoja 254 (Gósol), Mapa Geológico de España E. 1: 50.000. Segunda Serie (MAGNA)*. Madrid: IGME.

Mató, E., Martínez-Rius, A., Muñoz, J.A. & Escuer, J. (1994) *Hoja 293 (Berga), Mapa Geológico de España E. 1: 50.000. Segunda Serie (MAGNA)*. Madrid: IGME.

Miller, K.G., Kominz, M.A., Browning, J.V., Wright, J.D., Mountain, G.S., Katz, M.E., Sugarman, P.J., Cramer, B.S., Christie-Blick, N. & Pekar, S.F. (2005) The phanerozoic record of global sea-level change. *Science*, 310(5752), 1293–1298. https://doi.org/10.1126/science.1116412

Mochales, T., Barnolas, A., Pueyo, E.L., Serra-Kiel, J., Casas, A.M., Samsó, J.M., Ramajo, J. & Sanjuán, J. (2012) Chronostratigraphy of the Boltaña anticline and the Ainsa Basin (southern Pyrenees). *Bulletin Geological Society of America*, 124, 1229–1250. https://doi.org/10.1130/B30418.1

Molina, E., Alegret, L., Apellaniz, E., Bernaola, G., Caballero, F., Dinarès-turell, J., Hardenbol, J., Heilmann-Clausen, C., Larrasoaña, J.C., Luterbacher, H., Monechi, S., Ortiz, S., Orue-Etxebarria, X., Payros, A., Pujalte, V., Rodríguez-Tovar, F.J., Tori, F., Tosquella, J. & Uchman, A. (2011) The Global Stratotype Section and Point (GSSP) for the base of the Lutetian Stage at the Gorrondatxe section, Spain. *Episodes*, 34, 86–108. doi:10.18814/epiiugs/2011/v34i2/006

Moyà-Solà, S. & Kohler, M. (1993) Middle Bartonian locality with Anchomomys (Adapidae, Primates) in the Spanish Pyrenees: preliminary report. *Folia Primatologica*, 60, 158–163. https://doi.org/10.1159/000156684

Muñoz, J.A. (1992) Evolution of a continental collision belt: ECORS-Pyrenees crustal balanced cross-section. In: McClay, K.R. (Ed.) *Thrust tectonics*. Dordrecht: Springer, pp. 235–246. https://doi.org/10.1007/978-94-011-3066-0_21

Muñoz, J.A., Mencos, J., Roca, E., Carrera, N., Gratacós, O., Ferrer, O. & Fernández, O. (2018) The structure of the South-Central Pyrenean fold and thrust belt as constrained by subsurface data. *Geologica Acta*, 16, 439–460. 110.1344/GeologicaActa2018.16.4.7

Odlum, M.L., Stockli, D.F., Capaldi, T.N., Thomson, K.D., Clark, J., Puigdefàbregas, C. & Fildani, A. (2019) Tectonic and sediment provenance evolution of the South Eastern Pyrenean foreland basins during rift margin inversion and orogenic uplift. *Tectonophysics*, 765, 226–248. https://doi.org/10.1016/j.tecto.2019.05.008

Oms, O., Dinarès-Turell, J., Vicens, E., Estrada, R., Vila, B., Galobart, A. & Bravo, A.M. (2007) Integrated stratigraphy from the Vallcebre Basin (southeastern Pyrenees, Spain): new insights on the continental Cretaceous-Tertiary transition in southwest Europe. *Palaeogeography Palaeoclimatology Palaeoecology*, 255, 35–47. https://doi.org/10.1016/j.palaeo.2007.02.039

Oms, O., Fondevilla, V., Riera, V., Marmi, J., Vicens, E., Estrada, R., Anadon, P., Vila, B. & Galobart, A. (2016) Transitional environments of the lower Maastrichtian South-Pyrenean Basin (Catalonia, Spain): the Fumanya Member tidal flat. *Cretaceous Research*, 57, 428–442. https://doi.org/10.1016/j.cretres.2015.09.004

Payros, A., Pujalte, V. & Orue-Etxebarria, X. (1999) The South Pyrenean Eocene carbonate megabreccias revisited: new interpretation based on evidence from the Pamplona Basin. *Sedimentary Geology*, 125, 165–194. https://doi.org/10.1016/S0037-0738(99)00004-4

Puigdefàbregas, C., Muñoz, J.A. & Marzo, M. (1986) Thrust belt development in the Eastern Pyrenees and related depositional sequences in the southern Foreland Basin. In: Allen, P.A. &

Homewood, P. (Eds.) *Foreland Basins*. Barcelona: John Wiley & Sons, Ltd., pp. 229–246. https://doi.org/10.1002/9781444303810.ch12

Pujalte, V., Baceta, J.I., Schmitz, B., Orue-Etxebarria, X., Payros, A., Bernaola, G., Apellaniz, E., Caballero, F., Robador, A., Serra-Kiel, J. & Tosquella, J. (2009) Redefinition of the Ilerdian Stage (early Eocene). *Geologica Acta*, 7, 177–194. https://doi.org/10.1344/105.000000268

Ramos, E., Busquets, P. & Vergés, J. (2002) Interplay between longitudinal fluvial and transverse alluvial fan systems and growing thrusts in piggyback basin (SE Pyrenees). *Sedimentary Geology*, 146, 105–131. https://doi.org/10.1016/S0037-0738(01)00169-5

Riveline, J. (1986) *Les Charophytes du Paléogène et du Miocène Inférieur d'Europe Occidentale*. Paris: Cahiers de Paléontologie. Editions du C.N.R.S.

Rodríguez-Pintó, A., Pueyo, E.L., Serra-Kiel, J., Samsó, J.M., Barnolas, A. & Pocoví, A. (2012) Lutetian magnetostratigraphic calibration of larger foraminifera zonation (SBZ) in the Southern Pyrenees: the Isuela section. *Palaeogeography Palaeoclimatology Palaeoecology*, 333–334, 107–120. https://doi.org/10.1016/j.palaeo.2012.03.012

Rodríguez-Pintó, A., Serra-Kiel, J., Bernaola, G., Barnolas, A., Pueyo, E.L., Tosquella, J., Arbués, P. & Scholger, R. (2022) The early/middle Eocene transition at the Ésera valley (South-Central Pyrenees): implications in Shallow Benthic Zones (SBZ). *Geologica Acta*, 20(6), 1–25. 110.1344/GeologicaActa2022.20.6

Rosell, J. & Llompart, R.L.C. (2001) El 'garumniense' prepirenaico. *Revista de la Sociedad Geológica de España*, 14, 47–56.

Santolaria, P., Casas-Sainz, A.M., Soto, R. & Casas, A. (2016) Gravity modelling to assess salt tectonics in the western end of the South Pyrenean Central Unit. *Journal of the Geological Society*, 174, 269–288. https://doi.org/10.1144/jgs2016-027

Sclater, J.G. & Christie, P.A. (1980) Continental stretching: an explanation of the post-mid-Cretaceous subsidence of the Central North Sea Basin. *Journal of Geophysical Research*, 85, 3711–3739. https://doi.org/10.1029/JB085iB07p03711

Serra-Kiel, J., Hottinger, L., Caus, E., Drobne, K., Ferrandez, C., Jauhri, A.K., Less, G., Pavlovec, R., Pignatti, J., Samsó, J.M., Schaub, H., Sirel, E., Strougo, A., Tambareau, Y., Tosquella, J. & Zakrevskay, E. (1998) Larger foraminiferal biostratigraphy of the Tethyan Paleocene and Eocene. *Bulletin de la Société Géologique de France*, 169(2), 281–299.

Serra-Kiel, J., Travé, A., Mató, E., Saula, E., Ferràndez-Cañadell, C., Busquets, P., Tosquella, J. & Vergés, J. (2003) Marine and transitional Middle/Upper Eocene units of the southeastern Pyrenean foreland basin (NE Spain). *Geologica Acta*, 1(2), 177–200. https://doi.org/10.1344/105.000001609

Serra-Kiel, J., Vicedo, V., Baceta, J.I., Bernaola, G. & Robador, A. (2020) Paleocene larger foraminifera from the Pyrenean basin with a recalibration of the Paleocene Shallow Benthic Zone. *Geologica Acta*, 18, 1–70. https://doi.org/10.1344/GeologicaActa2020.18.8

Silva-Casal, R., Serra-Kiel, J., Rodríguez-Pintó, A., Pueyo, L.E., Aurell, M. & Payros, A. (2021) Systematics of Lutetian larger foraminifera and magnetobiostratigraphy from South Pyrenean Basin (Sierras Exteriores, Spain). *Geologica Acta*, 19(7), 1–64, I-XVII. https://doi.org/10.1344/GeologicaActa2021.19.7

Simó, A. & Puigdefàbregas, C. (1985) Transition from shelf to basin on an active slope, Upper Cretaceous, Tremp area, Southern Pyrenees. In: Mila, M.D. & Rosell, J. (Eds.) *IAS 6th European Regional Meeting, Excursion Guidebook*. Lerida, Spain: Instituto de Estudios Ilerdenses, pp. 63–108.

Solé Sugrañes, L. & Clavell, E. (1973) Nota sobre la edad y posición tectónica de los conglomerados eocenos de Queralt (Prepirineo oriental, Prov. de Barcelona). *Acta Geologica Hispánica*, 8, 1–6.

Soto, R., Casas, A.M., Sorti, F. & Faccenna, C. (2002) Role of lateral thickness variations on the development of oblique structures at the western end of the South Pyrenean Central Unit. *Tectonophysics*, 350, 215–235. https://doi.org/10.1016/S0040-1951(02)00116-6

Soulié-Märsche, I. (1971) Description de nouvelles charophytes éocènes. *Bulletin de la Société d'Histoire Naturelle de Toulouse*, 107, 18–27.

Steckler, M.S. & Watts, A.B. (1978) Subsidence of the Atlantic-type continental margin off New York. *Earth and Planetary Science Letters*, 41, 1–13. https://doi.org/10.1016/0012-821x(78)90036-5

Tauxe, L. & Watson, G.S. (1994) The fold test: an eigen analysis approach. *Earth and Planetary Science Letters*, 122, 331–341. https://doi.org/10.1016/0012-821X(94)90006-X

Tauxe, L., Kodama, K.P. & Kent, D.V. (2008) Testing corrections for paleomagnetic inclination error in sedimentary rocks: a comparative approach. *Physics of the Earth and Planetary Interiors*, 169, 152–165. https://doi.org/10.1016/j.pepi.2008.05.006

Tauxe, L., Shaar, R., Jonestrask, L., Swanson-Hysell, N.L., Minnett, R., Koppers, A.A.P., Constable, C.G., Jarboe, N., Gaastra, K. & Fairchild, L. (2016) PmagPy: software package for paleomagnetic data analysis and a bridge to the Magnetics Information Consortium (MagIC) Database. *Geochemistry, Geophysics, Geosystems*, 17, 2450–2463. https://doi.org/10.1002/2016GC006307

Teixell, A. (1998) Crustal structure and orogenic material budget in the west central Pyrenees. *Tectonics*, 17, 395–406. https://doi.org/10.1029/98TC00561

Tosquella, J. (1995) Els Nummulitinae del Paleocè-Eocè inferior de la conca sudpirinenca. PhD Thesis, Universitat de Barcelona.

Tosquella, J. & Samsó, J.M. (1996) Bioestratigrafía y litoestratigrafia del paleoceno superior-eoceno inferior del sector oriental de la cuenca surpirenaica. *Acta Geologica Hispánica*, 31, 3–21.

Ullastre, J., Durand-Delga, M. & Masriera, A. (1990) Relaciones tectónicas y sedimentarias entre la serie del Cadi y la zona del Pedraforca (Pirineo catalán). *Treballs del Museu de Geologia de Barcelona*, 1, 163–207.

Van Eeckhout, J.A., Giménez, J., Martínez, A., Mató, E., Ramos, E., Saula, E., Busquets, P., Colombo, F. & Permanyer, A. (1991) Variaciones Geométricas de la cuenca de antepaís surpirenaica relacionadas con los episodios de progradación-retrogradación de los sistemas deposicionales aluviales transicionales y marinos en la zona del Ripollès-Berguedà. In: Colombo, F. (Ed.) *I Congreso del Grupo Español del Terciario, Excuresion Guidebook n°3*.

van Hinsbergen, D.J.J., Torsvik, T.H., Schmid, S.M., Maţenco, L.C., Maffione, M., Vissers, R.L.M., Gürer, D. & Spakman, W. (2020) Orogenic architecture of the Mediterranean region and kinematic reconstruction of its tectonic evolution since the Triassic. *Gondwana Research*, 81, 79–229. https://doi.org/10.1016/j.gr.2019.07.009

Van Hinte, J.E. (1978) Geohistory analysis—application of micropaleontology in exploration geology. *AAPG Bulletin*, 62(2), 201–222. https://doi.org/10.1306/C1EA4815-16C9-11D7-8645000102C1865D

Vergés, J. (1993) Estudi geològic del vessant sud del Pirineu oriental i central. Evolució cinemàtica en 3D. PhD Thesis University of Barcelona, Monografia Tècnica 7, Servei Geològic de Catalunya, Barcelona.

Vergés, J., Martínez, A., Fleta, J., Pujadas, J., Tosquella, J., Samsó, J.M., Sanz, J., Barberà, M. & Beràstegui, X. (1994) *Memoria de la Hoja 255 (La Pobla de Lillet) Mapa Geológico de España E. 1:50.000 Segunda Serie (MAGNA)*. Madrid: IGME.

Vergés, J., Millan, H., Roca, E., Muñoz, J.A., Marzo, M., Cires, J., Den Bezemer, T., Zoetemeijer, R. & Cloetingh, S. (1995) Eastern Pyrenees and related foreland basins: pre-, syn- and post-collisional crustal-scale cross-sections. *Marine and Petroleum Geology*, 12, 903–915. https://doi.org/10.1016/0264-8172(95)98854-X

Vergés, J., Santaeulària, T., Serra-Kiel, J., Burbank, D.W., Muñoz, J.A. & Giménez-Montsant, J. (1998) Quantified vertical motions and tectonic evolution of the SE Pyrenean foreland basin. *Geological Society Special Publication*, 134, 107–134. https://doi.org/10.1144/gsl.sp.1998.134.01.06

Vergés, J., Fernàndez, M. & Martínez, A. (2002) The Pyrenean orogen: pre-, syn-, and post-collisional evolution. In: Rosenbaum, G. & Lister, G. (Eds.) *Reconstruction of the evolution of the Alpine-Himalayan orogen*, *Journal of the Virtual Explorer* 8. https://doi.org/10.3809/jvirtex.2002.00058

Vicente, A., Expósito, M., Sanjuan, J. & Martín-Closas, C. (2016) Small sized charophyte gyrogonites in the Maastrichtian of Coll de Nargó, Eastern Pyrenees: an adaptation to temporary floodplain ponds. *Cretaceous Research*, 57, 443–456. https://doi.org/10.1016/j.cretres.2015.07.017

Vicente, A., Csiki-Sava, Z. & Martín-Closas, C. (2019) European charophyte evolution across the Cretaceous–Paleogene boundary. *Palaeogeography Palaeoclimatology Palaeoecology*, 533, 109244. https://doi.org/10.1016/j.palaeo.2019.109244

Vinyoles, A., López-Blanco, M., Garcés, M., Arbués, P., Valero, L., Beamud, E., Oliva-Urcia, B. & Cabello, P. (2021) 10 Myr evolution of sedimentation rates in a deep marine to non-marine foreland basin system: tectonic and sedimentary controls (Eocene, Tremp–Jaca basin, Southern Pyrenees, NE Spain). *Basin Research*, 33, 447–477. https://doi.org/10.1111/bre.12481

SUPPORTING INFORMATION

Additional supporting information can be found online in the Supporting Information section at the end of this article.

How to cite this article: Juvany, P., Garcés, M., Lopez-Blanco, M., Martín Closas, C., Beamud Amorós, E., Tosquella, J. et al. (2024) Chronostratigraphy and tectono-sedimentary history of the Eastern South Pyrenean foreland basin (Ripoll Syncline, North-East Spain). *The Depositional Record*, 00, 1–26. Available from: https://doi.org/10.1002/dep2.287